



HAL
open science

PGI 2 Inhibits Intestinal Epithelial Permeability and Apoptosis to Alleviate Colitis

Camille Pochard, Jacques Gonzales, Anne Bessard, Maxime M Mahe, Arnaud Bourreille, Nicolas Cenac, Anne Jarry, Emmanuel Coron, Juliette Podevin, Guillaume Meurette, et al.

► **To cite this version:**

Camille Pochard, Jacques Gonzales, Anne Bessard, Maxime M Mahe, Arnaud Bourreille, et al.. PGI 2 Inhibits Intestinal Epithelial Permeability and Apoptosis to Alleviate Colitis. Cellular and Molecular Gastroenterology and Hepatology, 2021, 12 (3), pp.1037-1060. 10.1016/j.jcmgh.2021.05.001 . inserm-03287962v1

HAL Id: inserm-03287962

<https://inserm.hal.science/inserm-03287962v1>

Submitted on 16 Jul 2021 (v1), last revised 19 Aug 2021 (v2)

HAL is a multi-disciplinary open access archive for the deposit and dissemination of scientific research documents, whether they are published or not. The documents may come from teaching and research institutions in France or abroad, or from public or private research centers.

L'archive ouverte pluridisciplinaire **HAL**, est destinée au dépôt et à la diffusion de documents scientifiques de niveau recherche, publiés ou non, émanant des établissements d'enseignement et de recherche français ou étrangers, des laboratoires publics ou privés.



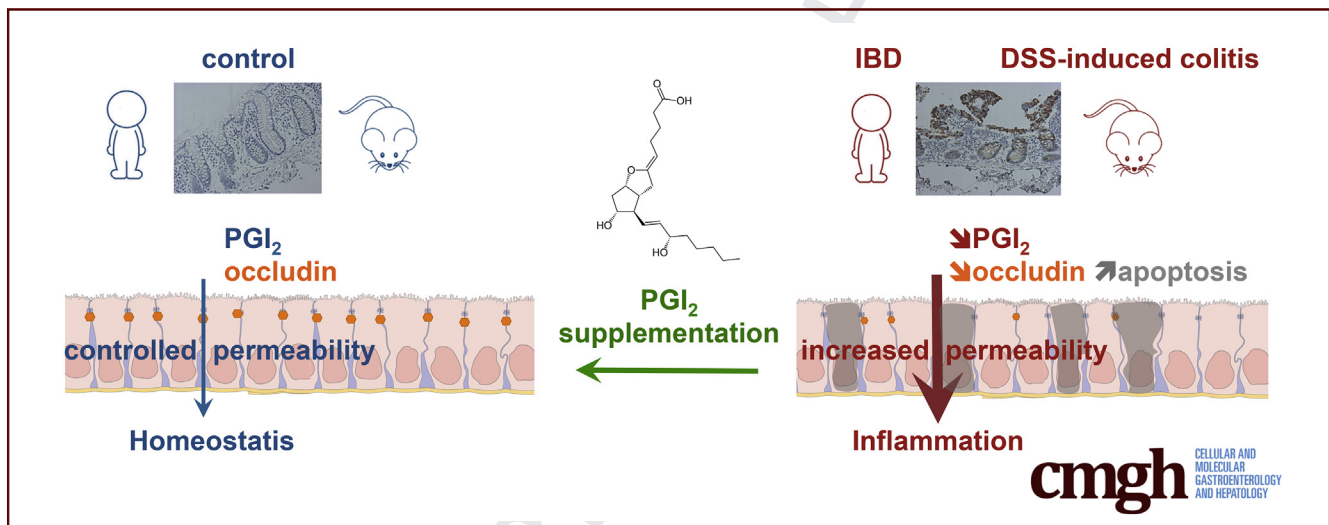
Distributed under a Creative Commons Attribution - NonCommercial - NoDerivatives 4.0 International License

ORIGINAL RESEARCH

PGI₂ Inhibits Intestinal Epithelial Permeability and Apoptosis to Alleviate Colitis

Camille Pochard,¹ Jacques Gonzales,¹ Anne Bessard,¹ Maxime M. Mahe,^{1,2,3} Arnaud Bourreille,^{1,4,5} Nicolas Cenac,⁶ Anne Jarry,⁷ Emmanuel Coron,^{1,4} Juliette Podevin,⁴ Guillaume Meurette,^{1,4} Michel Neunlist,¹ and Malvyne Rolli-Derkinderen¹

¹Université de Nantes, Inserm, TENS, The Enteric Nervous System in Gut and Brain Disorders, Institut des Maladies de l'Appareil Digestif, Nantes, France; ²Department of Pediatric General and Thoracic Surgery, Cincinnati Children's Hospital Medical Center, Cincinnati, Ohio; ³Department of Pediatrics, University of Cincinnati, Cincinnati, Ohio; ⁴CHU de Nantes, Hôpital Hôtel-Dieu, Nantes, France; ⁵CIC 1413, Nantes, France; ⁶UMR1220, IRSD, INSERM, INRA, INP-ENVT, Université de Toulouse, Toulouse, France; and ⁷Université de Nantes, Inserm, CRCINA, Nantes, France



SUMMARY

This study questions reduced prostacyclin production in mucosa from inflammatory bowel disease patients and highlights prostacyclin regulation of the intestinal epithelial barrier. Combining mouse model and human sample analyses, we demonstrated that prostacyclin prevented colitis and occludin down-regulation, inhibited apoptosis, induced occludin membrane location, and reduced intestinal epithelial permeability.

BACKGROUND & AIMS: Inflammatory bowel diseases (IBDs) that encompass both ulcerative colitis and Crohn's disease are a major public health problem with an etiology that has not been fully elucidated. There is a need to improve disease outcomes and preventive measures by developing new effective and lasting treatments. Although polyunsaturated fatty acid metabolites play an important role in the pathogenesis of several disorders, their contribution to IBD is yet to be understood.

METHODS: Polyunsaturated fatty acids metabolite profiles were established from biopsy samples obtained from Crohn's

disease, ulcerative colitis, or control patients. The impact of a prostaglandin I₂ (PGI₂) analog on intestinal epithelial permeability was tested in vitro using Caco-2 cells and ex vivo using human or mouse explants. In addition, mice were treated with PGI₂ to observe dextran sulfate sodium (DSS)-induced colitis. Tight junction protein expression, subcellular location, and apoptosis were measured in the different models by immunohistochemistry and Western blotting.

RESULTS: A significant reduction of PGI₂ in IBD patient biopsies was identified. PGI₂ treatment reduced colonic inflammation, increased occludin expression, decreased caspase-3 cleavage and intestinal permeability, and prevented colitis development in DSS-induced mice. Using colonic explants from mouse and human control subjects, the staurosporine-induced increase in paracellular permeability was prevented by PGI₂. PGI₂ also induced the membrane location of occludin and reduced the permeability observed in colonic biopsies from IBD patients.

CONCLUSIONS: The present study identified a PGI₂ defect in the intestinal mucosa of IBD patients and demonstrated its protective role during colitis. (*Cell Mol Gastroenterol Hepatol* 2021;■:■-■; <https://doi.org/10.1016/j.jcmgh.2021.05.001>)

Keywords: IBD; PGI₂; Caspase-3; Human Mucosa; Lipidomic; Occludin; Omega-6 (n-6).

Inflammatory bowel diseases (IBDs) that encompass both ulcerative colitis (UC) and Crohn's disease (CD) are complex chronic inflammatory disorders with increasing incidence and prevalence worldwide in the past decade.¹ IBD is now a major public health problem that affects approximately 3.6 million people in the United States and Europe.² IBD is characterized by chronic or relapsing immune activation and inflammation of the gastrointestinal (GI) tract that severely alter its function. Common IBD symptoms include bleeding, severe diarrhea, cramps, abdominal pain, fever, and weight loss. In CD as well as UC, inflammation of the gut is associated with breakdown of intestinal barrier integrity, abnormal secretions, and changes in motility patterns. Despite optimized use of immunosuppressive drugs and development of biotherapies, preventing disease relapse remains a challenge, and surgery is still required in approximately one-third of patients. Failure of approved therapies and in some cases the inability to provide a surgical treatment because of physical extension and/or mislocation of lesions are still major challenges to the management of IBD.^{3,4} In the absence of a definitive cure, better understanding of the pathophysiology of IBD is necessary to improve disease outcomes and prevention as well as to discover new effective and lasting treatments.

Although the etiology of IBD has not been fully elucidated, it is currently known that IBD pathogenesis is sustained by aberrant immune responses associated with changes in microbiota composition as well as alterations of the intestinal epithelial barrier (IEB).⁵ Numerous susceptibility loci as well as environmental risks factors have been described for CD and UC.^{2,6} Despite susceptibility genes that are for the most part different between CD and UC, 30% of IBD-related loci are common to these 2 intestinal diseases. These genes are involved in the immune system modulation, microbiota recognition, and most interestingly in the modulation of IEB functions (permeability, repair, autophagy).⁶ IEB-increased permeability has been described as an early feature of IBD,^{7,8} and its reduction protects against the development of inflammation.⁹ Moreover, increased intestinal permeability has been shown to precede the onset¹⁰ and relapse of CD^{11,12} as well as to occur in uninflamed areas.¹³ This suggests that intestinal permeability defects can occur irrespective of inflammation. In addition, intestinal mucosal healing is associated with clinical remission.^{14,15} Altogether, these events suggest that altered regulation of the IEB might contribute to IBD pathogenesis. Hence, strengthening of the IEB could be part of the therapeutic strategy.

Eicosanoids are potent bioactive signaling lipids derived from arachidonic acid and eicosapentaenoic acid. These polyunsaturated fatty acids (PUFAs) are associated with a diverse set of inflammatory processes linked to various

diseases including IBD. The production of some *n*-6 proinflammatory PUFA derivatives is increased in the lower GI tract of IBD patients compared with control subjects^{16–19} or in inflamed mucosa relative to non-inflamed mucosa^{20–23} and correlate with inflammation severity.²⁴ These findings support the idea of an imbalance between the *n*-6 proinflammatory and *n*-3 anti-inflammatory derivatives as pathologic contributing factors, but this concept was challenged when it has been found for several derivatives that they could have proinflammatory as well as anti-inflammatory properties.^{25–30} In addition, although most PUFA metabolites have been studied individually in an inflammatory context, it has been difficult to get a global view of lipid metabolic cascades that are involved in inflammation-related pathologies. More importantly, recent findings define the importance of pro-resolutive properties of some *n*-6 derivatives³¹ and their homeostatic functions.^{32,33} We recently reported that 2 eicosanoids, 15-hydroxyeicosatetraenoic acid (15-HETE) and prostaglandin (PG) 11 β -PGF_{2 α} , can respectively regulate IEB permeability³⁴ and healing.³⁵ They are down-regulated in CD,^{34,35} suggesting a pro-resolutive and pro-homeostatic function in IBD.

The current study presented a large profile of *n*-6 and *n*-3 PUFA-derived bioactive lipid mediators in the supernatant of human biopsies from both IBD and control patients using liquid chromatography coupled to tandem mass spectrometry. Within a cluster of bioactive lipid mediators down-regulated in IBD, PGI₂ was identified, and its effects on IEB functions were addressed. In particular, human IEB integrity and colitis development in a mouse model were assessed.

Results

6-ketoPGF_{1 α} (PGI₂ Metabolite), 11 β -PGF_{2 α} , and PGE₂ Are Decreased in Healthy Mucosa From IBD Patients

Using PUFA metabolite profiling from biopsy supernatants, metabolite production was determined in CD (n = 27) or UC (n = 19) versus control (n = 16) patients and in healthy areas (HA) versus unhealthy areas (UHA) in CD and UC patients. Cluster analysis of 23 detected metabolites in biopsy supernatants differentiated 3 clusters of

Abbreviations used in this paper: ANOVA, analysis of variance; CD, Crohn's disease; DAI, Disease Activity Index; DSS, dextran sulfate sodium; GI, gastrointestinal; HA, healthy area; 15-HETE, 15-hydroxyeicosatetraenoic acid; HRP, horseradish peroxidase; IBD, inflammatory bowel disease; IEB, intestinal epithelial barrier; IEC, intestinal epithelial cell; IFN, interferon; IL, interleukin; IP, prostaglandin I₂ receptor; MLC, myosin light chain; PBS, phosphate-buffered saline; PCNA, proliferating cell nuclear antigen; PG, prostaglandin; PUFA, polyunsaturated fatty acid; qPCR, real-time quantitative polymerase chain reaction; SEM, standard error of the mean; TEER, transepithelial electrical resistance; UC, ulcerative colitis; UHA, unhealthy area; ZO-1, zonula occludens.

© 2021 The Authors. Published by Elsevier Inc. on behalf of the AGA Institute. This is an open access article under the CC BY-NC-ND license (<http://creativecommons.org/licenses/by-nc-nd/4.0/>).

2352-345X

<https://doi.org/10.1016/j.jcmgh.2021.05.001>

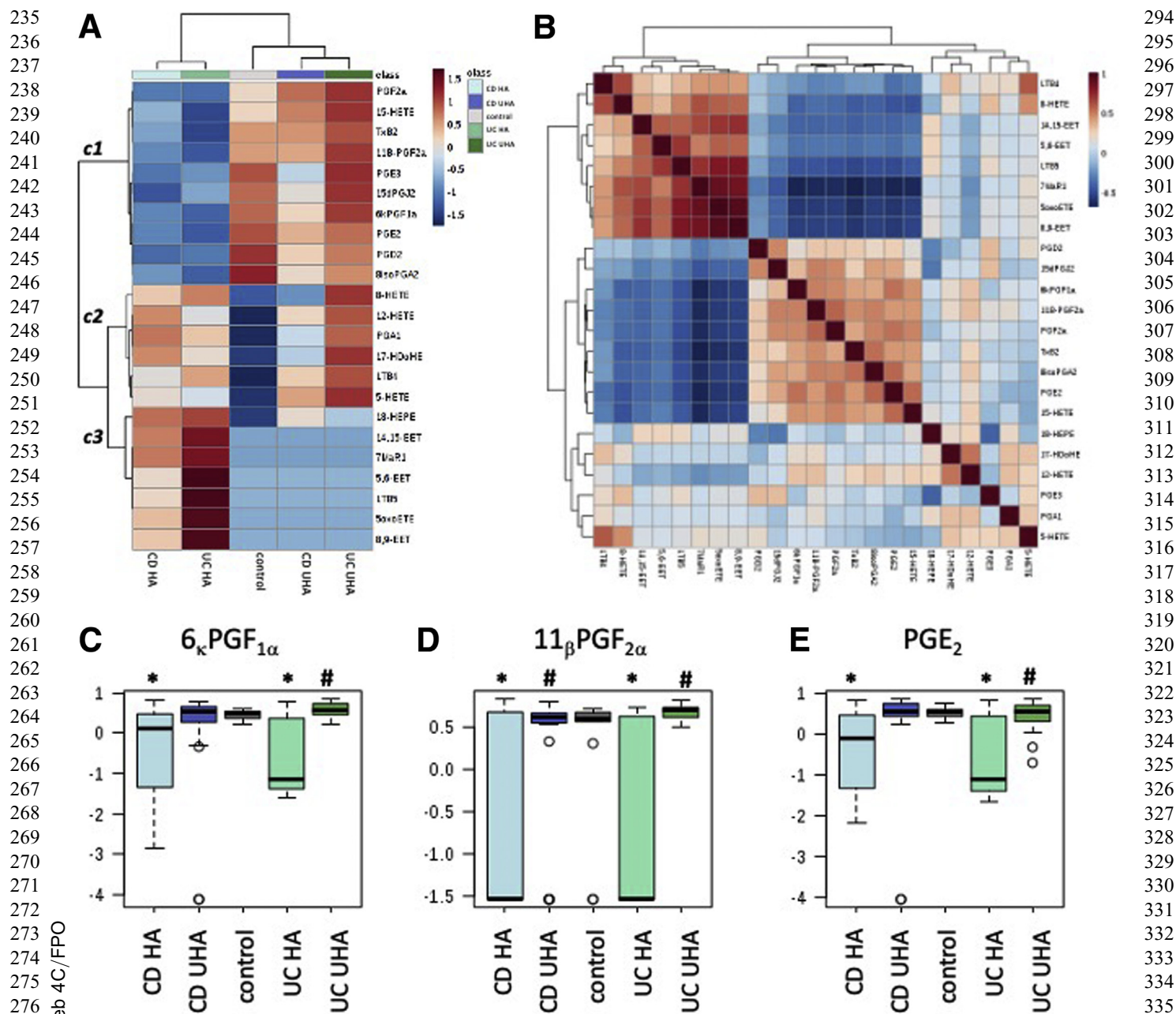


Figure 1. *n*-6/*n*-3 PUFA-derived metabolite profiling in biopsy supernatants from control and IBD patients. (A) Heatmap of mean concentrations of liquid chromatography–tandem mass spectrometry–identified PUFA metabolites in biopsy supernatants from control patients and HA and UHA of CD and UC patients. Color of each section is proportional to the fold-change of lipids (red, up-regulated; blue, down-regulated). Rows: metabolites; columns: patient groups. *c*1, *c*2, *c*3 indicate the 3 main clusters identified. (B) Correlation analysis of the differential metabolites (red, positive correlation factor; blue, negative correlation factor). (C–E) ANOVA analysis of 6-ketoPGF_{1α} (C, stable hydrolyzed product of unstable PGI₂), 11β-PGF_{2α} (D), and PGE₂ (E) levels in biopsy supernatants from control and HA and UHA of CD and UC patients. **P* ≤ .05 versus control; #*P* ≤ .05 UHA versus HA.

metabolites. The first cluster, *c*1, included 10 metabolites down-regulated in HA of CD and UC patients versus UHA and control patients (PGF_{2α}, 15-HETE, TxB₂, 11β-PGF_{2α}, PGE₃, 15-deoxyPGJ₂, 6-ketoPGF_{1α}, PGE₂, PGD₂, 8-isoPGA₂). The second cluster, *c*2, consisted of 6 up-regulated metabolites in HA and UHA of CD and UC patients versus control patients (8-HETE, 12-HETE, PGA₁, 17-HDoHE, LTB₄, 5-HETE). The last cluster, *c*3, included 7 up-regulated

metabolites in HA of CD and UC patients versus UHA or control patients (18-HEPE, 14,15-EET, 7-MaR1, 5,6-EET, LTB₅, 5-oxoETE, 8,9-EET) (Figure 1A, Figure 2A and B). Clustering of lipid profiles was not associated with patient treatments (Figure 3A and B). This cluster analysis revealed that a cluster of mediators was significantly reduced in HA of IBD patients when compared with control mucosa. Spearman correlation analysis showed a significant

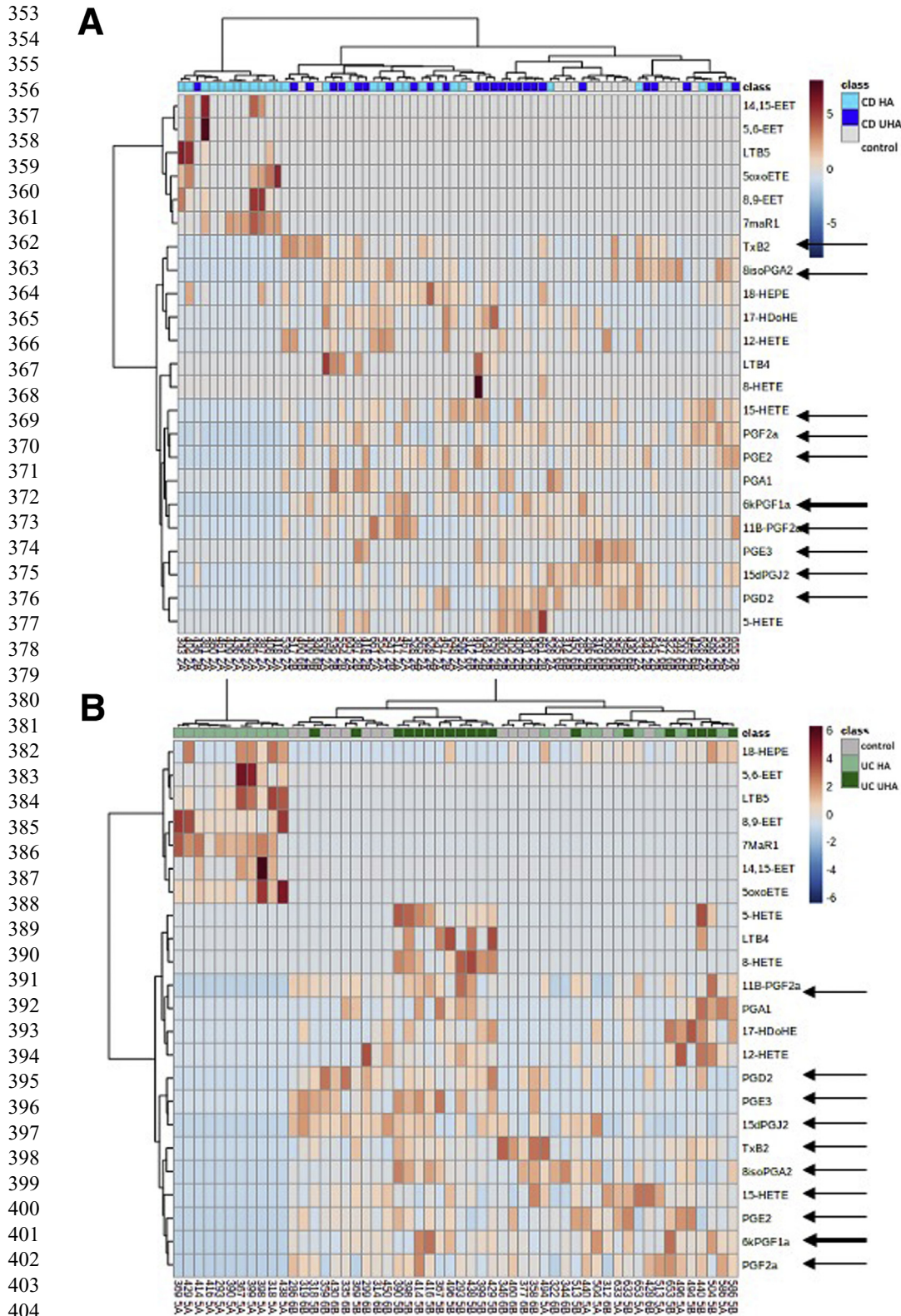


Figure 2. *n*-6/*n*-3 PUFA-derived metabolite profiling in biopsy supernatants from control and IBD patients. (A) Heatmap of individual concentrations of liquid chromatography-tandem mass spectrometry-identified PUFA metabolites in biopsy supernatants from control patients (Control) and HA and UHA of CD patients. (B) Heatmap of individual concentrations of liquid chromatography-tandem mass spectrometry-identified PUFA metabolites in biopsy supernatants from control patients (Control) and HA and UHA of UC patients. Color of each section is proportional to the fold-change of lipids (*red*, up-regulated; *blue*, down-regulated). *Rows*: metabolites; *columns*: patient identification numbers followed by group identification (2A = CD HA, 2B = CD UHA, 5A = UC HA, 5B = UC UHA, 6B = Control). *Arrows* highlight the metabolites of cluster *c1* identified by analysis of the pool of CD and UC data (Figure 1).

412
413
414
415
416
417
418
419
420
421
422
423
424
425
426
427
428
429
430
431
432
433
434
435
436
437
438
439
440
441
442
443
444
445
446
447
448
449
450
451
452
453
454
455
456
457
458
459
460
461
462
463
464
465
466
467
468
469
470

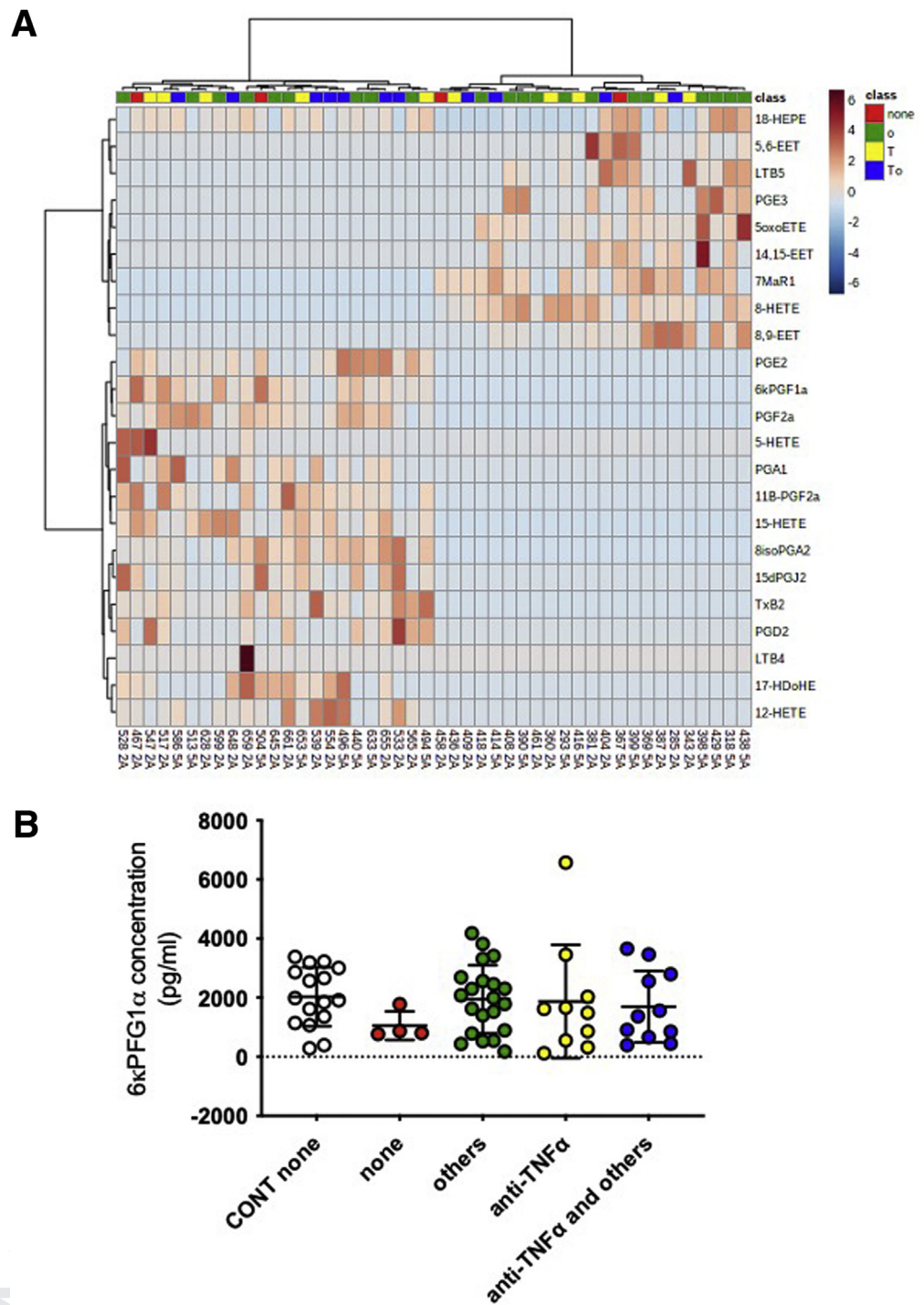
correlation with 9 metabolites from cluster *c1*, excluding only PGE₃ (Figure 1B). Interestingly, 5 of 9 correlated metabolites identified in cluster *c1* (15-HETE, 11β-PGF_{2α}, 15-

deoxyPGJ₂, PGD₂, PGE₂) are known to be involved in IEB integrity, a process that is altered in IBD. Therefore, these 9 mediators from cluster *c1* were focused on. Variance

471
472
473
474
475
476
477
478
479
480
481
482
483
484
485
486
487
488
489
490
491
492
493
494
495
496
497
498
499
500
501
502
503
504
505
506
507
508
509
510
511
512
513
514
515
516
517
518
519
520
521
522
523
524
525
526
527
528
529

Figure 3. n-6/n-3 PUFA-derived metabolite profiling in biopsy supernatants from IBD patients according to treatments.

(A) Heatmap of individual concentrations of liquid chromatography-tandem mass spectrometry-identified PUFA metabolites in biopsy supernatants from HA of CD and UC patients according to their treatments: no treatment (none), anti-tumor necrosis factor (TNF)- α treatment (T), other treatments (o, anti-inflammatory or immunosuppressive drugs), and anti-TNF- α combined with other treatments (To). Color of each section is proportional to the fold-change of lipids (red, up-regulated; blue, down-regulated). Rows: metabolites; columns: patient identification numbers followed by group identification (2A = CD HA, 5A = UC HA). (B) ANOVA analysis of 6-ketoPGF_{1 α} (C, stable hydrolyzed product of unstable PGI₂) concentrations in biopsy supernatants from control untreated patients (CONT none) and CD and UC patients without treatment (none), treated with anti-TNF- α , anti-inflammatory, or immunosuppressive drugs (others), and anti-TNF- α combined with other treatments (anti-TNF- α and others).



530
531
532
533
534
535
536
537
538
539
540
541
542
543
544
545
546
547
548
549
550
551
552
553
554
555
556
557
558
559
560
561
562
563
564
565
566
567
568
569
570
571
572
573
574
575
576
577
578
579
580
581
582
583
584
585
586
587
588

analyses demonstrated that the concentrations of 6-ketoPGF_{1 α} (Figure 1C), 11 β -PGF_{2 α} (Figure 1D), and PGE₂ (Figure 1E) were significantly lower in HA of CD or UC patients compared with control patients. In addition, their concentrations were significantly increased in UHA versus HA for UC patients (Figure 1C-E). Although 11 β -PGF_{2 α} and PGE₂ involvement in IEB regulation has been described,^{35,36} the role of PGI₂ (6-ketoPGF_{1 α} is the stable, inactive metabolite of the bioactive PGI₂) is yet to be known. Thus, focus was centered on PGI₂ regulation of

intestinal permeability and its putative role in IEB defects observed in IBD patients.

PGI₂ Decreases Caco-2 Monolayer Permeability

To investigate PGI₂ effects on IEB, whether the PGI₂ analog iloprost can directly modulate the resistance and permeability of Caco-2 intestinal epithelial cell (IEC) monolayers in vitro was assessed. This PGI₂ analog significantly increased the transepithelial electrical resistance

(TEER) (Figure 4A) and decreased paracellular permeability of Caco-2 monolayers compared with untreated cells (Figure 4B). Iloprost significantly regulated permeability when applied to the basolateral but not when applied to the apical side (Figure 4J).³⁷ To ensure that the observed effects were not mediated by the inactive PGI₂ degradation product 6-ketoPGF_{1α}, the TEER and permeability of Caco-2 cells treated with 6-ketoPGF_{1α} were also measured. Both TEER (Figure 4K) and permeability (Figure 4L) remained unchanged. These data demonstrate that PGI₂ can directly regulate IEB resistance and permeability.

PGI₂ Increases Occludin and Decreases Claudin-2 and Zonula Occludens-1 Expression In Vitro

To investigate the mechanisms of PGI₂ regulation of IEB permeability, expression of tight junction proteins and regulators of paracellular permeability in Caco-2 cells treated or untreated with iloprost was assessed. Zonula occludens-1 (ZO-1) and claudin-2 expression were significantly decreased in the presence of iloprost (Figure 4C-E). In contrast, occludin expression was significantly increased by iloprost treatment (Figure 4C and F). Junctional adhesion molecule-A, cingulin, and phosphorylated myosin light chain (MLC) 20 expressions were unchanged by iloprost treatment (Figures 4C and G-I). These data showed that PGI₂ analog treatment modified tight junction protein expression.

PGI₂ Inhibits Dextran Sulfate Sodium-Induced Colitis and Prevents Increased Permeability and Mucosal Destruction In Vivo

To study the role of PGI₂ in vivo, the damage observed in dextran sulfate sodium (DSS)-induced mouse colitis model was examined with or without synthetic PGI₂ epoprostenol treatment (Figure 5A). The typical weight loss observed in DSS-induced mice was absent when they received PGI₂ (Figure 5B). As expected, the Disease Activity Index (DAI), which considers stool consistency and gross bleeding, significantly increased in DSS-induced mice compared with control animals and significantly decreased in PGI₂-treated mice compared with DSS-induced colitis mice (Figure 5C). To assess the impact of PGI₂ supplementation on IEB integrity, intestinal permeability was measured in vivo. Paracellular permeability was increased in DSS-induced mice compared with control animals, and PGI₂ treatment reduced the DSS-induced permeability to baseline levels (Figure 5E). Transcellular permeability was unaffected between all 4 experimental groups (Figure 5D). Both the cecal atrophy and reduction of colon length observed in DSS-treated mice were prevented when these mice simultaneously received PGI₂ (Figure 3F and G). Epoprostenol injections in control mice did not affect the measured parameters (Figure 3B-G). The DSS-induced changes in distal colon morphology were also prevented by PGI₂ treatment (Figure 5I). Quantification of this intestinal remodeling showed that PGI₂ treatment prevented mucosal architecture alteration (Figure 5H) but did not prevent muscle thickening (Figure 5J). Mucosal infiltration by immune cells and goblet cell depletion were only significantly

increased in DSS-induced colitis mice compared with control mice without PGI₂ treatment (Figure 5K and L). Altogether, these data showed a beneficial role of PGI₂ supplementation that prevented intestinal damage observed in vivo during colitis development induced by DSS.

PGI₂ Partially Reduces Inflammation Observed in DSS-Induced Colitis

The effect of PGI₂ on the colonic inflammatory response induced by DSS with or without synthetic PGI₂ epoprostenol treatment was investigated next. DSS-induced increases in tumor necrosis factor- α (Figure 6A), interleukin (IL) 6 (Figure 6C), and IL17A (Figure 6E) mRNA expression were not affected by PGI₂ treatment. In contrast, DSS-induced increases in IL1 β (Figure 6B), interferon (IFN- γ) (Figure 6D), and IL22 (Figure 6F) mRNA expression were not significant when animals were treated with PGI₂. These data suggested that PGI₂ partially tampers with the inflammatory process via down-regulation of cytokines such as IL22, IFN- γ , and IL1 β .

PGI₂ Protects Against DSS-Induced Decreases in Occludin Expression and Apoptosis

To investigate the molecular remodeling associated with PGI₂ effects on IEB during colitis development, expressions of occludin and claudin-2, the 2 tight junction proteins identified in Caco-2 cells (Figure 4), were analyzed in mice colons. Occludin immunostaining showed clear epithelial staining unchanged by PGI₂ supplementation. DSS-induced colitis decreased occludin staining that was restored by PGI₂ treatment (Figure 7A and C). Because IEB permeability could be regulated by changes in tight junction protein expression as well as modulation of IEC apoptosis or renewal, cleaved caspase-3 expression, proliferating cell nuclear antigen (PCNA) expression, and Akt phosphorylation in the colon of DSS-induced mice with or without PGI₂ treatment were measured. Immunofluorescent staining revealed a higher level of cleaved caspase-3 in the colonic mucosa of DSS-induced colitis mice compared with controls, mice treated with PGI₂ alone, and DSS-induced mice treated with PGI₂ (Figure 7B and D). PCNA expression was not modified (Figure 7E and F), but Akt phosphorylation was increased in DSS-induced mice treated with PGI₂ compared with PGI₂-treated animals (Figure 7E and G). These data suggested that in addition to maintenance of occludin expression, PGI₂ can play an epithelial protective role by decreasing apoptosis and promoting IEC survival.

PGI₂ Inhibits Apoptosis and Permeability and Induces Membrane-Associated Occludin Expression in Human and Mouse Explants Ex Vivo

To validate PGI₂ ability to prevent IEB permeability induced by altered tight junction proteins and epithelial apoptosis, colonic samples from control mice and mucosal explants from control patients treated with the apoptosis inducer staurosporine were treated with or without iloprost, and permeability was measured in Ussing chambers. Mice

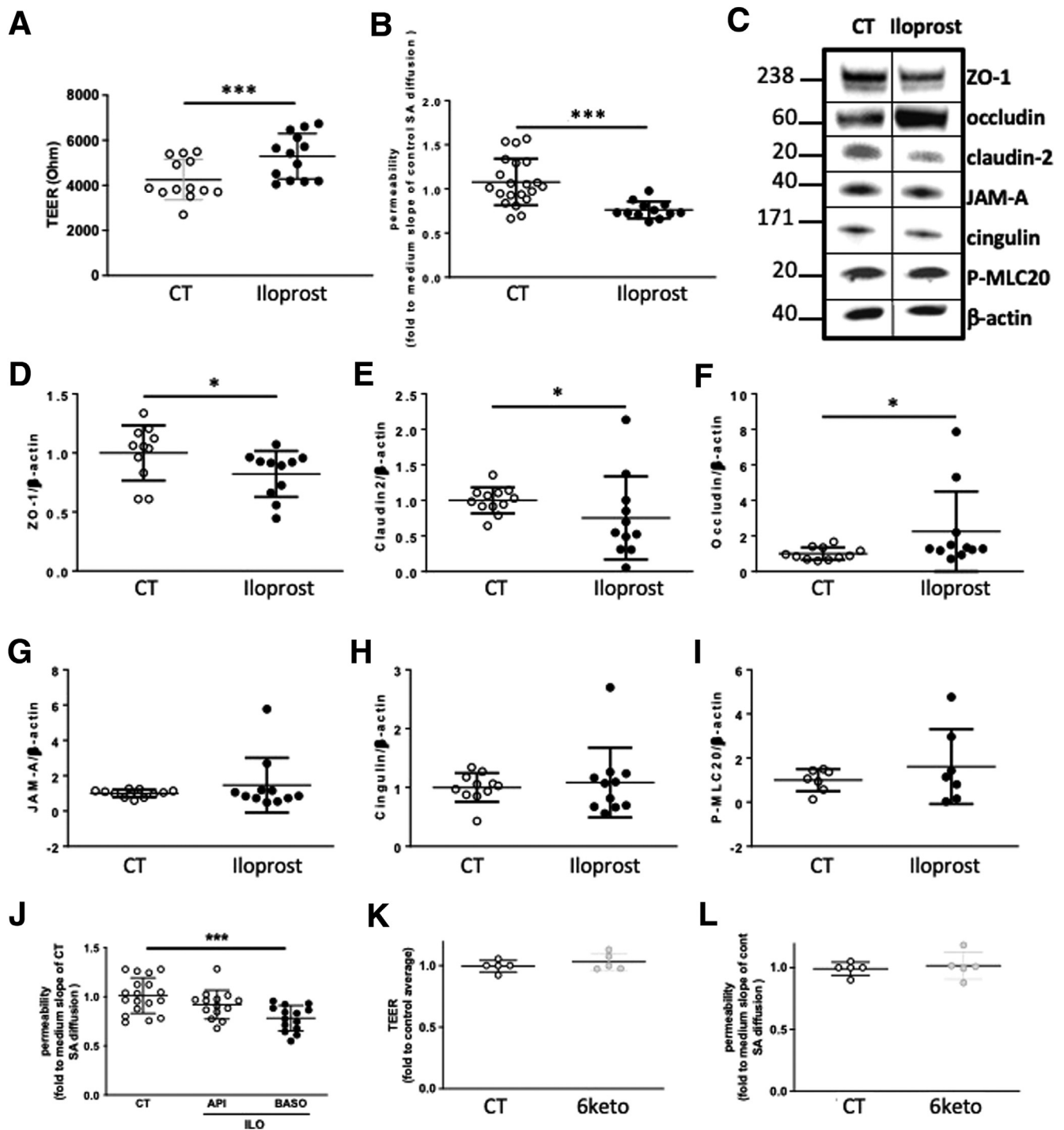
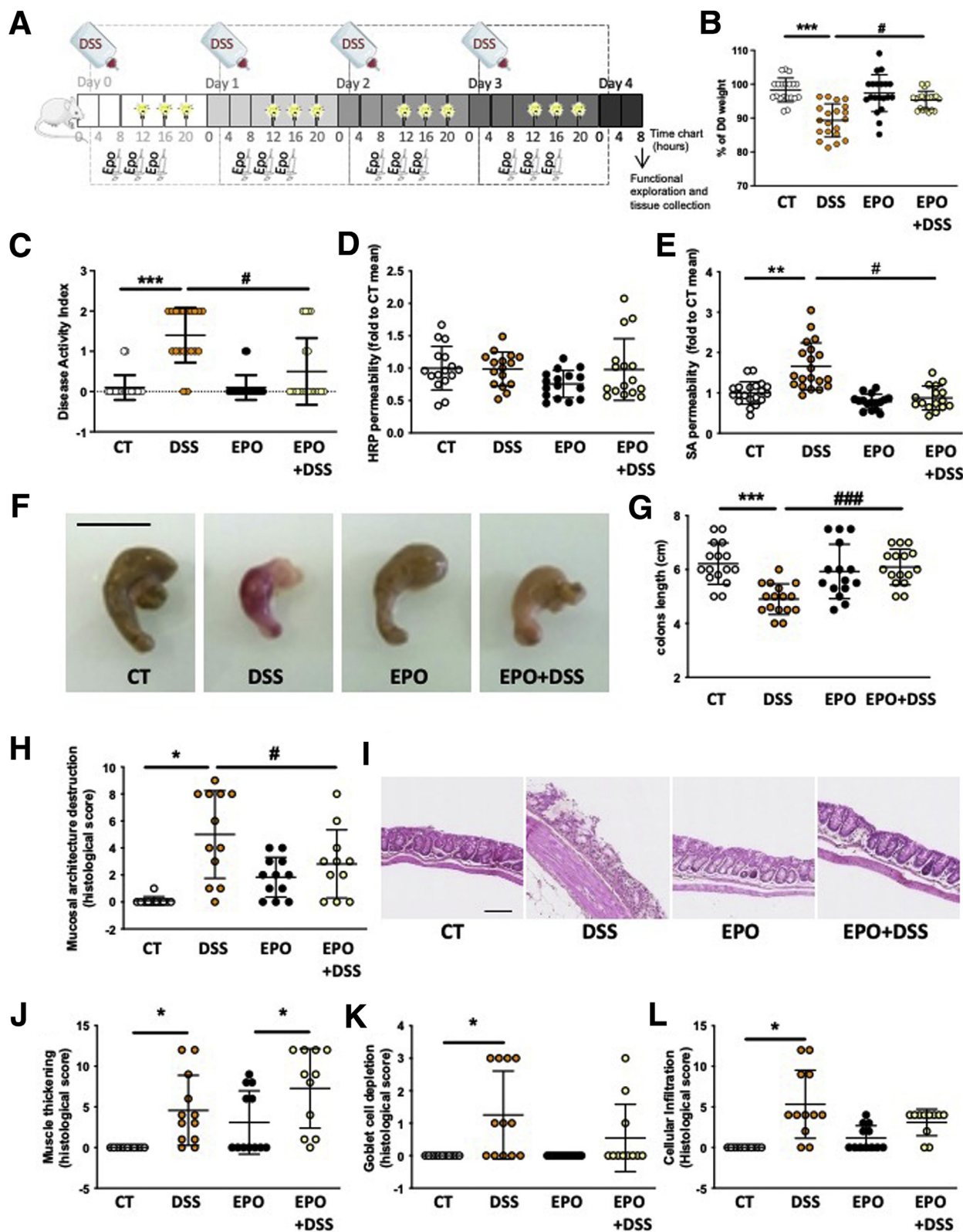


Figure 4. PGI₂ analog iloprost increases resistance, reduces permeability, increases occludin, and decreases ZO-1 and claudin-2 expression in vitro. (A and B) PGI₂ impact on TEER (A) and permeability (B) was measured in vitro on Caco-2 monolayer after 1 day with or without (CT) 10 μ mol/L iloprost in the basolateral compartment. Data represent means \pm SEM of 13–16 Caco-2 filters per condition. *** P < .001 Mann-Whitney test. (C–I) Western blot analyses of tight junction protein expression from Caco-2 lysates. Representative Western blot (C), ZO-1 (D), claudin-2 (E), occludin (F), junctional adhesion molecule-A (G), cingulin (H), and phosphorylated MLC20 (I) expression quantification related to β -actin expression from Western blot analysis. In (D–I), data represent means \pm SEM of 7–12 Caco-2 filters per condition. * P \leq .05 nonparametric Mann-Whitney test. (J) Sulfonic acid permeability was measured on Caco-2 monolayer after 1 day of 10 μ mol/L iloprost (ILO) treatment in basolateral (Baso) or apical (Api) compartments or without it (Cont). (K) TEER was measured on Caco-2 monolayer after 1 day of 10 μ mol/L 6-ketoPGF_{1 α} (6 keto) treatment in the basolateral compartment or without it (Cont). (L) Paracellular permeability was measured by sulfonic acid (SA) flux through the same Caco-2 monolayer. Data represent means \pm SEM of 3–6 independent experiments. * P > .05 by nonparametric Mann-Whitney test.

825 explants treated with staurosporine showed an increased
826 cleaved caspase-3 level and apoptosis score (Figure 8A and D)
827 associated with a decrease in occludin expression (Figure 8B),
828 mucosal architecture disorganization (Figure 8C), and

increased permeability (Figure 8E). Supplementation with
the PGI₂ analog iloprost prevented all these changes
(Figure 8A–E). Dose-response experiments demonstrated
that 1 μmol/L iloprost had no significant effect (Figure 9A).

884
885
886
887
888
889
890
891
892
893
894
895
896
897
898
899
900
901
902
903
904
905
906
907
908
909
910
911
912
913
914
915
916
917
918
919
920
921
922
923
924
925
926
927
928
929
930
931
932
933
934
935
936
937
938
939
940
941
942



Cell fractionation analyses showed that rather than an increase in total occludin expression, iloprost increased membrane-associated occludin (Figure 9B and C). In human explants, staurosporine treatment also increased paracellular permeability that was entirely inhibited by iloprost supplementation, leading to a recovery of permeability values (Figure 10A). Altogether, these data demonstrated that iloprost was able to prevent apoptosis-induced permeability. Cleaved caspase-3 expression increased within 2–5 hours after staurosporine treatment. This effect was again entirely inhibited by iloprost pretreatment (Figure 10B).

Apoptosis and Cleaved Caspase-3 Expression Are Increased in the Mucosa of CD and UC Patients

To determine whether apoptosis was increased in the mucosa of IBD patients, apoptosis was measured by (1) immunohistochemistry using an antibody directed to cleaved caspase-3 or the cytochrome c antibody specific for apoptotic epithelial cells³⁸ and (2) measuring *BAX* and *BCL2* mRNA expression in the mucosa of control, CD, and UC patients. Whereas the expression of cleaved caspase-3 was increased in CD and UC patients compared with control patients (Figure 10C and D), *BCL2* and *BAX* mRNA were unchanged (Figure 10E and F). Immunohistochemistry of cleaved caspase-3 and epithelial apoptosis measurement using cytochrome c antibody showed very low levels of cleaved caspase-3⁺ or cytochrome c⁺ cells in control patients, whereas high numbers of both were observed in CD or UC patients (Figure 10C). These data indicate that epithelial apoptosis was increased in the mucosa of CD and UC patients compared with control patients. To determine how tight junction proteins are expressed in biopsies from IBD patients and whether it is dependent on disease activity, ZO-1 and occludin expressions in biopsies from control, quiescent, or active (HA and UHA) CD patients were analyzed. Whereas ZO-1 expression was not significantly altered (Figure 10H), occludin expression was significantly decreased in UHA of CD patients compared with HA or control biopsies (Figure 10I).

PGI₂ Reduces Permeability of Biopsies From IBD Patients

To assess whether PGI₂ treatment can reduce the increased permeability observed in IBD patients, biopsies from CD or UC patients were pretreated with the PGI₂

analog iloprost 1 hour before paracellular permeability measurement in Ussing chambers. Iloprost treatment significantly decreased the permeability of IBD biopsies (Figure 11A). This decrease was not due to altered expression of ZO-1 or occludin (Figure 11B) or the PGI₂ receptor (IP) in the mucosa of IBD patients because *IP* mRNA levels were not significantly different in CD or UC versus control mucosa (Figure 9G). Nevertheless, cell fractionation and immunohistochemistry analyses showed that occludin membrane expression increased when biopsies were treated with iloprost (Figure 11C–E). These results showed that PGI₂ can reduce the permeability of IBD biopsies, suggesting that the functional defect of PGI₂ mucosal production by IBD patients could be fixed by addition of a PGI₂ analog.

Discussion

Whereas IEB integrity loss is a well-recognized IBD contributing factor,³⁹ the underlying molecular mechanisms of IEB failure and strategies dedicated to protect and/or improve IEB remain to be identified. Not only does the current work give a clear picture of lipid metabolic profiles in human samples and better define the role of PGI₂ in IEB homeostasis, it also aids the understanding of *n*-6 PUFA-metabolite contributions to IBD development and proposes its use as an IEB reinforcing agent in IBD.

Our current findings first highlight a cluster of *n*-6 PUFA metabolites that are less present in supernatants of HA from CD or UC patients compared with UHA or control patients. This cluster is composed of 4 principal bioactive PGs (PGD₂, PGE₂, PGF_{2α}, PGI₂), 2 PGD₂ metabolites (11β-PGF_{2α}, 15-deoxyPGJ₂), thromboxane A₂, and 1 eicosanoid (15-HETE). It is important to note that their concentrations are decreased in non-inflamed HA but increased in inflamed UHA, which is consistent with the increased PG production generally induced by acute inflammation⁴⁰ and already observed in rectal mucosa of active UC patients,^{19,41,42} inflamed esophageal mucosa,⁴³ or experimental ileitis.⁴⁴ Nevertheless, genome-wide analysis of DNA methylation identified the down-regulation of the PGI₂ synthase in fibrotic CD patients,⁴⁵ reinforcing the idea that the decrease in PGI₂ content observed in HA of CD or UC patients herein could sensitize IEB and participate in IBD development.

The deleterious effect of PG defects reported in studies using PG inhibition has long been described in intestinal mucosa, not in IBD but through observations of gastric mucosal erosion and small intestine lesions induced by

Figure 5. (See previous page). Synthetic PGI₂ epoprostenol prevents DSS-induced colon atrophy, animal weight loss, and mucosal destruction and increases permeability in vivo. (A–E) PGI₂ impact on colitis induced by DSS in vivo was measured at end of the protocol in control (CT) or DSS-induced mice (DSS) that received PBS (NT) or epoprostenol (EPO) during the 4 days of the protocol. Experimental design (A), animal weight (B), DAI (C), transcellular permeability (D), and paracellular permeability (E) (evaluated by measurement of HRP and sulfonic acid in animal plasma 4 hours after mouse gavage), cecal remodeling (F; scale bar: 1 cm), and colon length (G). (H–L) Tissue remodeling was analyzed in the 4 groups of mice. Hematein Phloxin Safran coloration of distal colon sections of control (CT), DSS-induced (DSS), epoprostenol-treated (EPO), or epoprostenol-treated DSS-induced (EPO+DSS) mice (I; scale bar: 100 μm). Histologic scores were evaluated from Hematein Phloxin Safran staining by quantifying the destruction of mucosal architecture (H), muscle thickening (J), loss of goblet cells (K), and cellular infiltration (L). Data represent mean ± SEM of 4–12 mice per group. Two-way ANOVA followed by Bonferroni post hoc tests. **P* ≤ .05 and ****P* ≤ .001 (DSS factor effects) or #*P* ≤ .001 and ###*P* ≤ .001 (EPO factor effects).

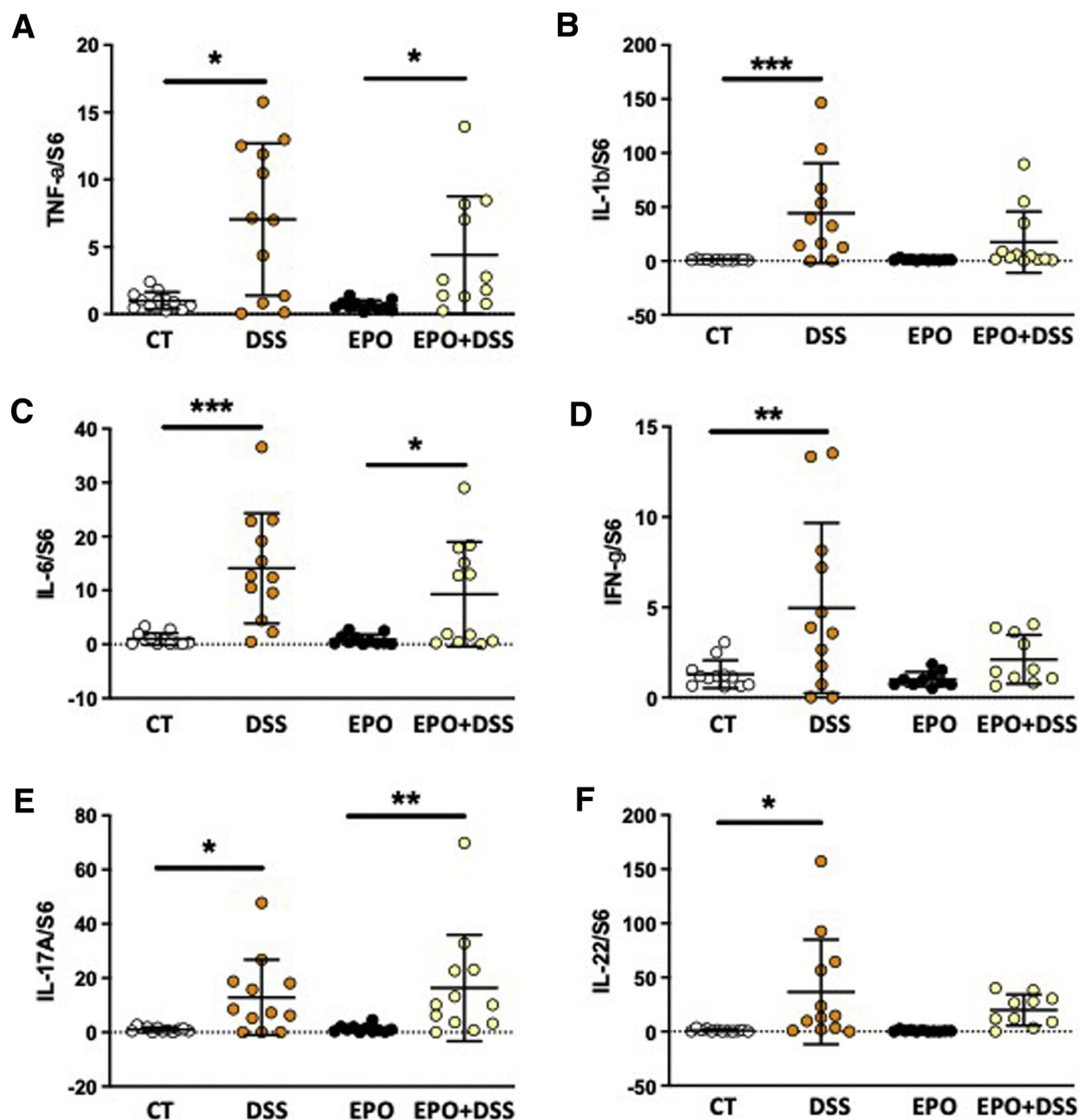


Figure 6. Synthetic PGI₂ epoprostenol partially prevents inflammation observed during colitis development. (A–F) mRNA expression of tumor necrosis factor (*Tnf*)- α (A), *IL-1 β* (B), *IL-6* (C), *IFN- γ* (D), *IL-17A* (E), and *IL-22* (F) was measured at end of 4-day treatment in colon fragments of control (CT) or DSS-induced mice (DSS) that received PBS (NT) or epoprostenol (EPO) every day. Data represent means \pm SEM of 12 mice per group. Two-way ANOVA followed by Bonferroni post hoc tests. * $P \leq .05$, ** $P \leq .01$, and *** $P \leq .001$ (DSS factor effects).

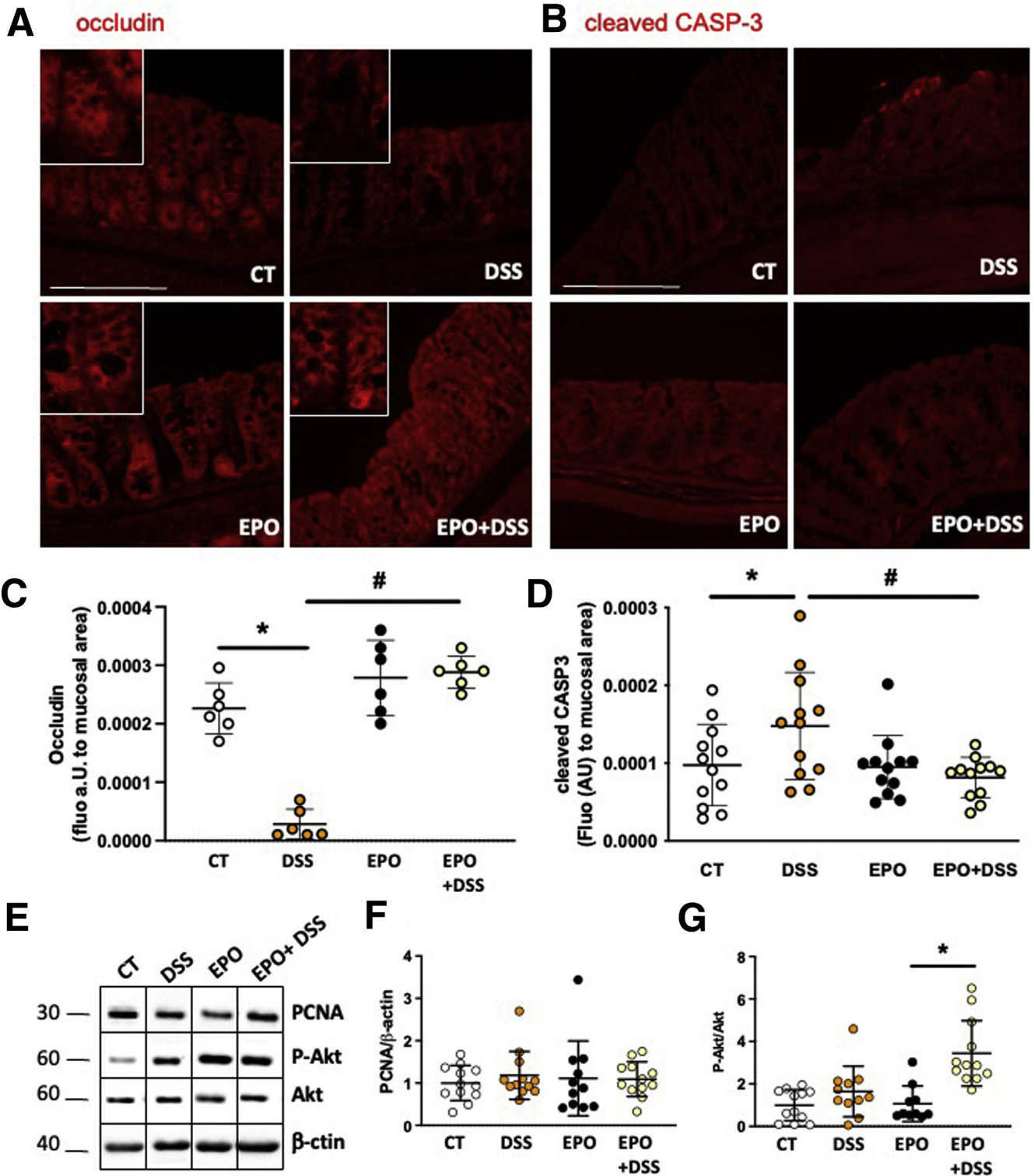
cyclooxygenase inhibition.⁴⁶ A decrease in endogenous gastric prostanoid synthesis has also been observed in ulcers,^{47–49} and the beneficial impact of PG supplementation on intestinal mucosa was described in the 1980s, particularly through the concept of cytoprotection developed by André Robert. He and others described how PG can prevent induction of gastric mucosal erosion and mainly concerns PGE₂.^{50,51} Numerous works have described PGE₂ effects in the GI tract, driving the current idea that PGE₂-specific

effects depend on the targeted receptor (EP1–4) and cell type and could provide mucosal protection to colitis through EP4/2 receptors.^{36,52,53} Concerning PGD₂, how its metabolites, 11 β -PGF_{2 α} and 15-deoxyPGJ₂, increase IEB healing³⁵ and modulate epithelial cell proliferation and differentiation has already been described.⁵⁴ Nevertheless, the role of PGD₂ in gut inflammation remains debated since Hokari et al²⁷ suggested that L-PGD synthase plays a proinflammatory role in the development of colitis in clinical and

1179 experimental studies. On the other hand, PGD₂/DP1 axis
 1180 activation has been shown to confer anti-inflammatory
 1181 properties^{26,29} and reduce colitis development.²⁸

1182 As for the other PG, PGI₂'s impact on gut function is
 1183 manifold and complex because it regulates and is produced
 1184 by different cell types, but its regulation of IEC function is
 1185 not well-described. Indeed, we know that PGI₂ regulates
 1186

1238 gastric emptying and small intestinal transit⁵⁵ through
 1239 regulation of smooth muscle contraction.⁵⁶⁻⁵⁹ PGI₂ is a well-
 1240 known vasodilator,⁶⁰ inhibitor of platelet aggregation,⁶¹ and
 1241 promoter of angiogenesis,⁶² and it is precisely through these
 1242 vascular effects that PGI₂ has a remarkable action against
 1243 anastomotic leakage under artificially obstructive condi-
 1244 tions,⁶³ could enhance colon anastomotic healing,⁶⁴ or
 1245



1297 improve intestinal barrier function.⁶⁵ Its well-described
1298 impact on the IEB itself includes reduction of acid secretion,
1299 ^{66,67} induction of chloride secretion,^{68,69} and inhibition
1300 of water and solute absorption.^{70,71} Concerning PGI₂ regu-
1301 lation of IEC proliferation or apoptosis, studies are contra-
1302 dictory. PGI₂ promotes HT29 cell proliferation in vitro⁷² but
1303 does not stimulate growth of gastroduodenal mucosa
1304 in vivo.⁶⁷ It does not impact HT29 apoptosis⁷² but promotes
1305 colonocyte survival and presents some anti-apoptotic effects
1306 through peroxisome proliferator-activated receptor δ acti-
1307 vation.⁷³ A working hypothesis is that these effects partici-
1308 pate in the increased restitution of IEC6 or Caco-2 cells⁷⁴
1309 and increased IEB restoration and resistance induced by
1310 PGI₂ when paired with PGE₂.⁷⁵⁻⁷⁸

1311 Our present work provides evidence that PGI₂ regulates
1312 intestinal epithelial permeability as well as tight junctions
1313 and has anti-apoptotic properties. We demonstrated that
1314 in vitro treatment of intestinal epithelial monolayers or
1315 isolated mouse or human mucosa explants with the PGI₂-
1316 stable analog iloprost decreases IEB permeability, increases
1317 occludin membrane expression, and protects against
1318 apoptosis. These effects could have been attributed to the
1319 activation of other eicosanoid pathways, because iloprost is
1320 not entirely selective for the PGI₂ receptor (IP) but could
1321 activate PGE₂ EP1-4 receptors.⁷⁹ Nevertheless, similar ef-
1322 fects were found using the synthetic PGI₂ epoprostenol,
1323 which can activate EP3 and more specifically the IP.⁸⁰
1324 Indeed, the present study demonstrated that PGI₂ supple-
1325 mentation in vivo inhibits DSS-induced colitis by decreasing
1326 induced epithelial permeability, maintaining occludin
1327 expression, and inhibiting epithelial apoptosis. Altogether,
1328 our findings show that PGI₂ is able to strengthen the IEB
1329 and suggest that this strengthening contributes to allevia-
1330 tion of colitis in vivo.

1331 Interestingly, the IEB properties improved by PGI₂ are
1332 deficient in IBD patients in whom increased permeability
1333 has been explained by defects in tight junction function or
1334 IEC renewal. In CD as well as UC, claudin-2 up-regulation,
1335 MLC kinase activation, or occludin down-regulation have
1336 already been observed.⁸¹ In addition to the regulation of
1337 permeability by tight junction proteins that occurs when the
1338 epithelium is intact, epithelial cell death can also cause
1339 barrier loss regardless of tight junction function.⁸² It has
1340 already been shown that lipopolysaccharide-induced
1341 apoptosis causes an increase in IEB paracellular
1342

1356 permeability⁸³ and that cleaved caspase-3 is associated with
1357 increased permeability in other colitis models.⁸⁴ After 4
1358 days of DSS treatment, an increase in cleaved caspase-3
1359 expression in the colon of the current colitis-mouse model
1360 was observed. This cleavage is consistent with the increase
1361 in cleaved caspase-3 observed in tissues from IBD patients
1362 that also presented higher epithelial apoptosis. Because
1363 changes in *BCL2* or *BAX* mRNA expression in the mucosa of
1364 CD or UC patients were not observed herein, it could be
1365 hypothesized that the transduction pathway leading to
1366 apoptosis is mainly an extrinsic one concerning IEC death
1367 receptor pathway activation. Moreover, the PGI₂ analog
1368 iloprost was demonstrated to efficiently inhibit apoptosis-
1369 induced permeability as well as permeability observed in
1370 IBD patient biopsies. This strongly suggests that the func-
1371 tional defect of PGI₂ mucosal production in IBD patients
1372 could be fixed by additional treatment with a PGI₂ analog.
1373 Whereas PGI₂ involvement in IEB homeostasis and func-
1374 tions was sparse, our work identified a decrease in PGI₂
1375 content in intestinal mucosa from IBD patients and clearly
1376 demonstrated that PGI₂ can directly target the IEB to
1377 decrease apoptosis and colitis-induced IEB permeability. In
1378 addition, the observation that PGI₂ supplementation
1379 decreased cellular infiltration as well as *IL22* and *IL1 β*
1380 expression in vivo in the DSS-induced colitis model suggests
1381 a more global modulatory effect of PGI₂, not only on
1382 epithelial but also on immune homeostasis. This idea is
1383 supported by the link and common mechanisms between
1384 IBD and chronic airway diseases⁸⁵ and the current wide-
1385 spread use of stable PGI₂ analogs beraprost and iloprost as
1386 treatment for pulmonary hypertension. These analogs
1387 showed potent anti-inflammatory and endothelium-
1388 dependent anti-edemagenic effects in several models of
1389 acute lung injury.⁸⁶ Nevertheless, investigation of PGI₂
1390 supplementation impact on immune cells and vascular
1391 functions remains to be completed before considering
1392 whether targeting the PGI₂ pathway may be therapeutically
1393 relevant in IBD.

1395 Methods

1396 Study Approval

1397 Patients provided written informed consent to take part
1398 in the study, and all procedures were performed according
1399 to the guidelines of the French Ethics Committee for
1400

1401
1402
1403
1404
1405
1406
1407
1408
1409
1410
1411
1412
1413
1414

Figure 7. (See previous page). Synthetic PGI₂ epoprostenol inhibits decreased occludin expression and apoptosis induced by DSS in vivo. (A and C) PGI₂ impact on occludin expression. Representative occludin immunostaining of distal colon sections of control (CT), DSS-induced (DSS), epoprostenol-treated (EPO), or epoprostenol-treated and DSS-induced (EPO+DSS) mice at end of 4-day treatment (A; scale bar: 100 μ m). Occludin mucosa staining was quantified in the 4 groups of mice (C). (B and D) PGI₂ impact on apoptosis. Representative cleaved caspase-3 immunostaining of distal colon sections of control (CT), DSS-induced (DSS), epoprostenol-treated (EPO), or epoprostenol-treated and DSS-induced (EPO+DSS) mice at end of 4-day treatment (B). Quantification of cleaved caspase-3 staining relative to mucosal area in the 4 groups of mice (D). Data represent means \pm SEM of 4 mice per group. Two-way ANOVA followed by Bonferroni post hoc tests. * $P < .05$ (DSS factor effects) or # $P < .05$ (EPO factor effects). (E-G) Western blot analyses of PCNA, phospho-Akt (P-Akt), and Akt were performed on the distal colon of control (CT), DSS-induced (DSS) epoprostenol-treated (EPO), or epoprostenol-treated and DSS-induced (EPO+DSS) mice at end of 4-day treatment. Representative Western blot analysis of PCNA and P-Akt/Akt expression (E). Quantification of PCNA expression (F). Quantification of P-Akt/Akt expression derived from acquisition of the same gels (G). Data represent means \pm SEM of 12 mice per group. Two-way ANOVA followed by Bonferroni post hoc tests. * $P \leq .05$ (DSS factor effects) or # $P \leq .05$ (EPO factor effects).

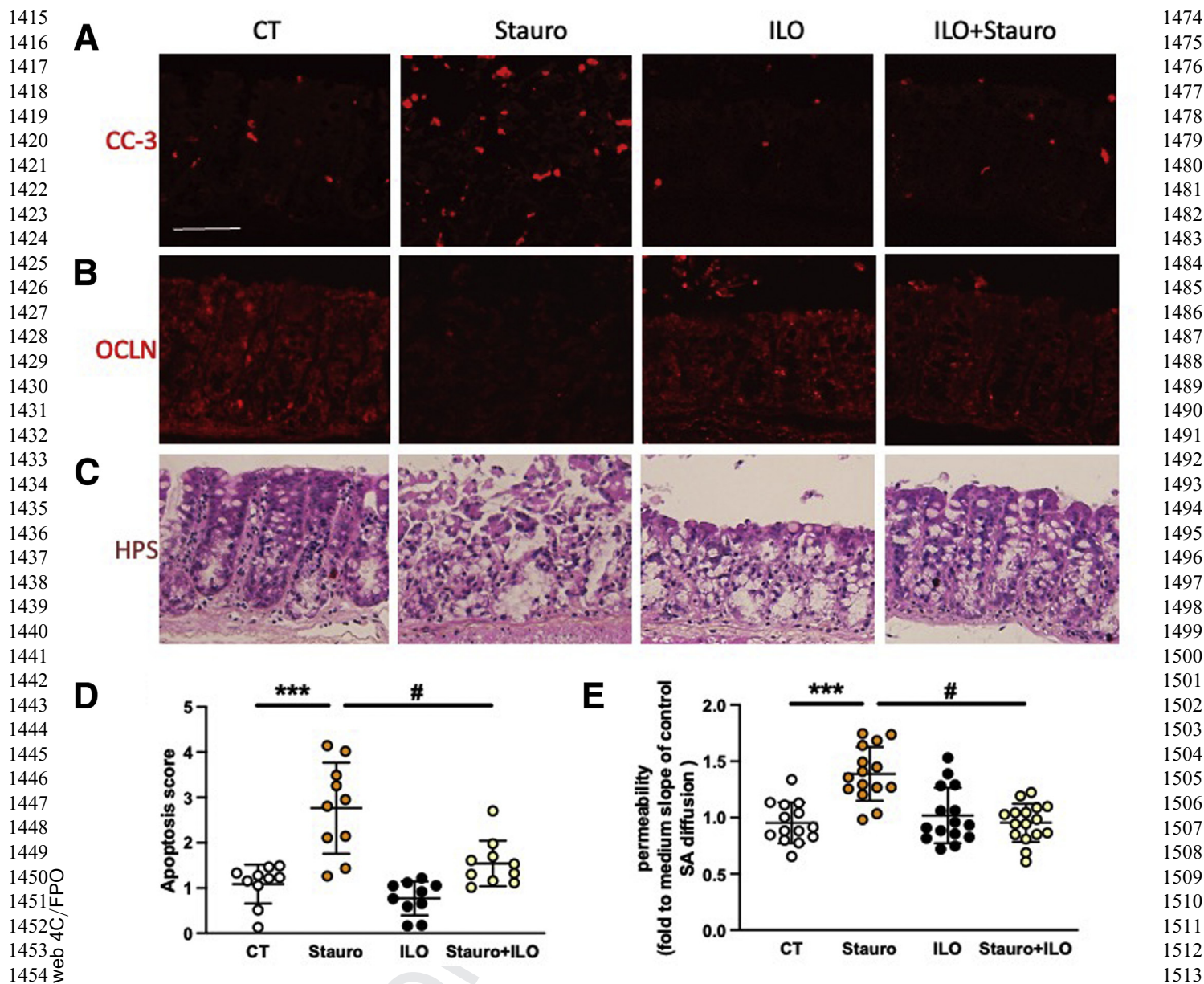


Figure 8. PGI₂ analog iloprost prevents mouse IEB breakdown ex vivo. (A–D) Potential of PGI₂ to block IEB breakdown induced by apoptosis was assessed on mouse colon explants treated without (CT) or with staurosporine (Stauro, 1 μmol/L) for 20 hours, without or with 4-hour pretreatment with 10 μmol/L iloprost pretreatment (ILO). Representative cleaved caspase-3 (CC3, A), occludin (OCLN, B), or Hematein Phloxin Safran staining (HPS, C) of explants from proximal colon of mice after the mentioned treatments (scale bar: 50 μm). Apoptosis score evaluated from cleaved caspase-3 staining (D). Paracellular permeability measured in Ussing chambers by sulfonic acid flux through mouse tissues after the mentioned treatments (E). Data represent means ± SEM of 16 explants per group. Two-way ANOVA followed by Bonferroni post hoc tests. ****P* ≤ .001 (for DSS factor effects) or #*P* ≤ .05 (for ILO factor effects).

Research on Humans and registered under no. DC-2008-402. All experiments involving mice were approved by the Ethics Committee for Animal Experimentation of Pays de la Loire (study no. 01953.01).

Patients

Human tissues originating from control, CD, or UC patients were used for biopsy supernatant analyses (Table 1), mucosa explants (Table 2), mucosa histology,

molecular analyses (Table 3), and biopsy permeability analyses (Table 4). Briefly, surgical resections (used for explants and mucosa analyses) were collected from macroscopically and microscopically unaffected fragments from patients undergoing surgery. Control patients were those undergoing surgery for colon cancer except 2 who were undergoing surgery for stenosis or Hartmann's procedure that were used for explants. Samples were always taken at least 10 cm away from the tumor. Biopsies were taken in macroscopically UHA and/or HA. Whereas

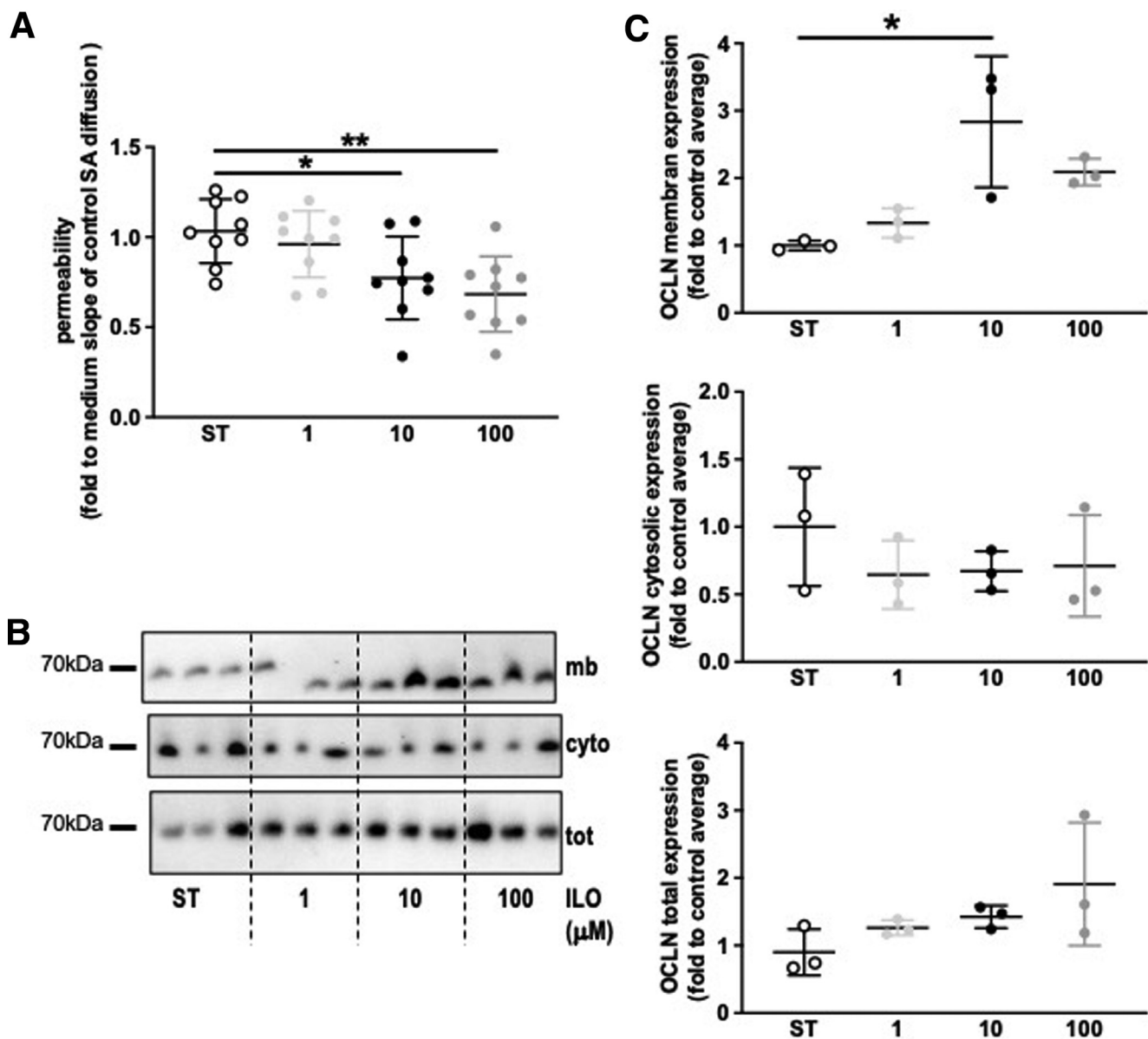


Figure 9. Dose response of PGI₂ analog iloprost on mice colon explant permeability and occludin membrane location. (A–C) Potential of PGI₂ to regulate occludin and reduce IEB permeability induced by apoptosis was assessed on mouse colon explants treated for 16 hours with staurosporine (ST, 1 $\mu\text{mol/L}$), without or with 4-hour pretreatment with 1, 10, or 100 $\mu\text{mol/L}$ iloprost (ILO). Paracellular permeability measured in Ussing chambers by sulfonic acid flux through mouse tissues after the mentioned treatments (A). Occludin membrane (mb), cytosolic (cyto), and total (tot) expression were assessed by Western blot after cell fractionation (B) and quantified (C). Data represent means \pm SEM of 3–9 explants per group. Nonparametric Mann-Whitney test, ** $P < .005$ or * $P < .05$.

surgical resections came from patients with severe forms of IBD, biopsies came from patients with light to moderate clinical forms of IBD (Mayo UC-DAI from 0 to 8; Harvey-Bradshaw Index from 0 to 7). The location of the samples and main clinical features of patients are mentioned in Tables 1–4.

Biopsy Supernatants

On removal, biopsies were rapidly weighed and immersed in hard plastic tubes containing 1 mL Hank's buffered saline solution per 10 mg biopsy sample and

continuously oxygenated (95% O₂/5% CO₂) at 37°C. After a 20-minute incubation, the solution was removed and centrifuged at 200g for 10 minutes before being filtered with centrifuge tube filters (0.22 μm , SPIN-X) to remove bacterial components. Supernatant aliquots (200 μL) were stored at –80°C until assayed.

PUFA Metabolite Profiling

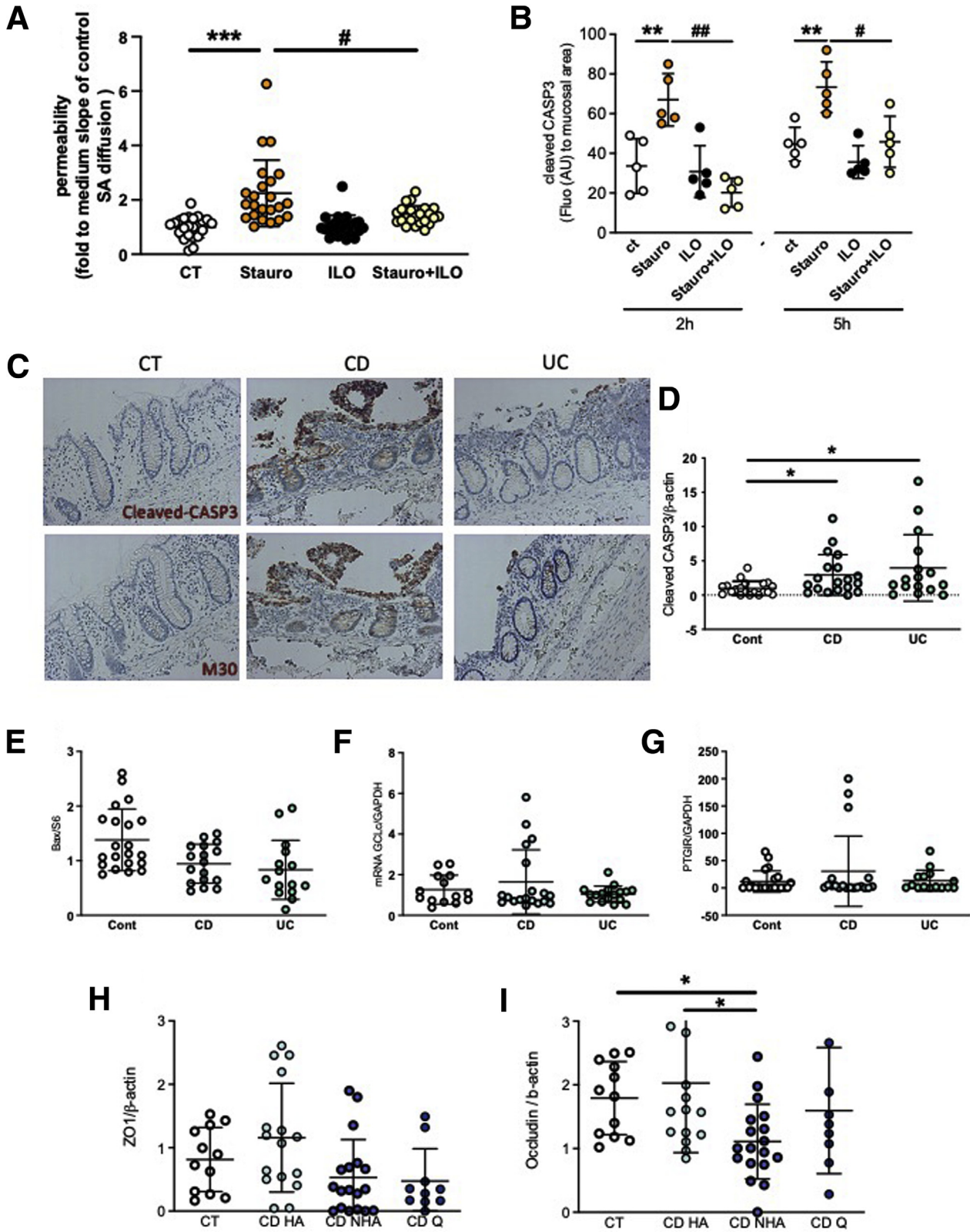
n-6/*n*-3 PUFA-derived metabolite dosages were performed as described by Le Faouder et al⁸⁷ from biopsy supernatants.

1651 **Data Preprocessing and Analysis**

1652 Data preprocessing was performed using the Metabo-
 1653 analyst web interface (www.metaboanalyst.ca).⁸⁸ Briefly,
 1654 preprocessing of the data matrix (concentrations) was

performed by removing missing values. The data matrix was
 transformed using a generalized logarithm and scaled using
 autoscaling method (mean-centering and division by the
 standard deviation of each variable). Heatmap and

1710
1711
1712
1713
1714
1715
1716
1717
1718
1719
1720
1721
1722
1723
1724
1725
1726
1727
1728
1729
1730
1731
1732
1733
1734
1735
1736
1737
1738
1739
1740
1741
1742
1743
1744
1745
1746
1747
1748
1749
1750
1751
1752
1753
1754
1755
1756
1757
1758
1759
1760
1761
1762
1763
1764
1765
1766
1767
1768



1769 hierarchical clustering presenting group averages and
1770 metabolite z-scores was performed on both samples and
1771 features using a Pearson distance measure and average
1772 clustering. The heatmap and correlation of metabolites were
1773 done using a Spearman rank correlation distance measure.
1774 The pattern hunter was performed on 6-ketoPGF_{1α} with a
1775 Pearson distance measure. One-way analysis of variance
1776 (ANOVA) was calculated with an adjusted *P* value cutoff of
1777 .05 and a Fisher least significant difference post hoc test.

1779 Human Explants

1780 Human explants were obtained from human colon
1781 samples (Table 2) washed with cold Krebs's solution and
1782 from which the muscle layers and submucosa were
1783 removed. Mucosa explants (30–40 mg) were maintained in
1784 culture in RPMI/Ham's F12 medium (v/v) supplemented
1785 with 0.01% bovine serum albumin, 100 IU/mL penicillin,
1786 and 100 μg/mL streptomycin and fungizone (1%) at 37°C
1787 with 95% O₂ and 5% CO₂ under gentle agitation. Explants
1788 were incubated with 10 μmol/L iloprost 4 hours before
1789 addition of 1 μmol/L staurosporine. After 18 hours in cul-
1790 ture, explants were placed in Ussing chambers for perme-
1791 ability measurement.

1794 Mucosa Histology and Molecular Analyses

1795 Human surgical resections (Table 3) were washed
1796 with cold Krebs's solution, and then the mucosa was
1797 removed and fixed for 1 hour in 4% paraformaldehyde
1798 solution or snap frozen for further analysis (immuno-
1799 staining or real-time quantitative polymerase chain reac-
1800 tion [qPCR]).

1802 Biopsy Permeability

1803 On removal, biopsies were placed in Ussing chambers
1804 and incubated with 10 μmol/L iloprost 1 hour before
1805 permeability measurement.

1808 Caco-2 Culture, TEER, and Permeability 1809 Measurement In Vitro

1810 The human IEC line Caco-2 was obtained from American
1811 Type Culture Collection (Manassas, VA) and cultured in

1828 Dulbecco modified Eagle medium containing 4.5 g/L glucose
1829 (Gibco, Life Technologies, Carlsbad, CA) supplemented with
1830 10% heat-inactivated fetal calf serum, 2 mmol/L glutamine,
1831 100 IU/mL penicillin, and 100 μg/mL streptomycin. For
1832 TEER and permeability experiments, 100,000 Caco-2 cells
1833 were seeded onto 24-well Transwell filters coated with
1834 collagen I. The metabolite 6-ketoPGF_{1α} (10 μmol/L; Cayman
1835 Chemical Co, Ann Arbor, MI) or 10 μmol/L iloprost (Cayman
1836 Chemical Co), 100 ng/mL epoprostenol (GlaxoSmithKline,
1837 Brentford, UK, or Panpharma, Luitre-Dompierre, France), or
1838 solvent was added the following day in the basolateral
1839 compartment. To determine the effect of 6-ketoPGF_{1α} or
1840 iloprost on IEB resistance, the TEER was measured 1 day
1841 after treatment with an epithelial voltohmmeter (EVOM;
1842 World Precision Instruments, Inc, Sarasota, FL). To deter-
1843 mine the effect of these same drugs on IEB permeability, 50
1844 μL of the apical medium was replaced by 50 μL fluo-
1845 rescein-5.6 sulfonic acid (1 mg/mL; Invitrogen, Carlsbad,
1846 CA). The fluorescence level of basolateral aliquots (150 μL)
1847 was measured every 30 minutes for a period of 180 minutes
1848 using a fluorimeter (Varioskan; Thermo SA, France). Para-
1849 cellular permeability was determined by averaging the slope
1850 change in fluorescence intensity over time by linear
1851 regression fit model.

1854 DSS-Induced Colitis and In Vivo Permeability 1855 Assessment

1856 Colitis was induced in 8-week-old male C57BL/6NRJ
1857 mice (Janvier Labs, Le Genest-Saint-Isle, France) by adding
1858 4% (w/v) DSS (MP Biomedicals, Santa Ana, CA) to the
1859 drinking water, which was renewed every day for 4 days.
1860 For in vivo assessment of PGI₂ effect, epoprostenol (1 μg/
1861 mL in phosphate-buffered saline [PBS]) or vehicle (PBS;
1862 given in 3 intraperitoneal injections of 100 μL at the
1863 beginning, middle, and end of the light cycle) (Figure 3A).
1864 Four mice per cage were subjected to a 12-hour light/12-
1865 hour dark cycle with free access to food (Safe, Augy,
1866 France) and water. Animals were weighed daily; on the
1867 last day, animals received 120 μL of a solution containing
1868 300 mg red carmine, 50 mg fluorescein-5.6 sulfonic acid,
1869 50 mg horseradish peroxidase (HRP) (Sigma-Aldrich, St
1870 Louis, MO), and 5 mL 0.5% carboxymethylcellulose by

1812
1813
1814 **Figure 10. (See previous page). PGI₂ analog iloprost prevents human IEB breakdown ex vivo, and mucosa from IBD**
1815 **patients present increased apoptosis and reduced occludin expression. (A and B)** Potential of PGI₂ to block IEB
1816 breakdown induced by apoptosis was assessed on human colon explants treated without (CT) with staurosporine (Stauro,
1817 1 μmol/L) for 20 hours (A) and the indicated time (B), without or with 4-hour 10 μmol/L iloprost pretreatment (ILO). Paracellular
1818 permeability measured in Ussing chambers by sulfonic acid flux through human mucosal colonic samples from control pa-
1819 tients after the mentioned treatment (A). Data represent means ± SEM of 6 explants per condition and per patient with 4
1820 different patients. Quantification of cleaved caspase-3 staining relative to mucosal area was quantified in 5 explants per group
1821 (B). Two-way ANOVA followed by Bonferroni post hoc tests. ****P* < .001 (for Stauro factor effects), ***P* < .05 (for Stauro factor
1822 effects), or **P* < .05 (for ILO factor effects). (C–F) Epithelial apoptosis was evaluated in mucosa from control (CT), CD, or UC
1823 patients by Western blot analysis, immunostaining, or qPCR. Representative immunostaining of cleaved caspase-3 or cyto-
1824 death M30 from CT, CD, and UC patients (C; scale bar: 200 μm). Quantification of cleaved caspase-3 normalized to β-actin
1825 expression observed by Western blot (D). Measurement of *BAX* (E), *BCL2* (F), and *PTGIR* (G) mRNA. Data represent means ±
1826 SEM of mucosa lysates from CT (n = 20), CD (n = 20), and UC (n = 16) patients. Nonparametric Mann-Whitney test, **P* < .05.
1827 (G and H) Quantification of ZO-1 (H) and occludin (I) expression normalized to β-actin expression observed by Western blot of
1828 biopsies from control, quiescent CD, and active CD HA and UHA. Data represent means ± SEM of mucosa lysates from CT
1829 (n = 12), active CD (n = 16), and quiescent CD (n = 9) patients. Nonparametric Mann-Whitney test, **P* < .05.

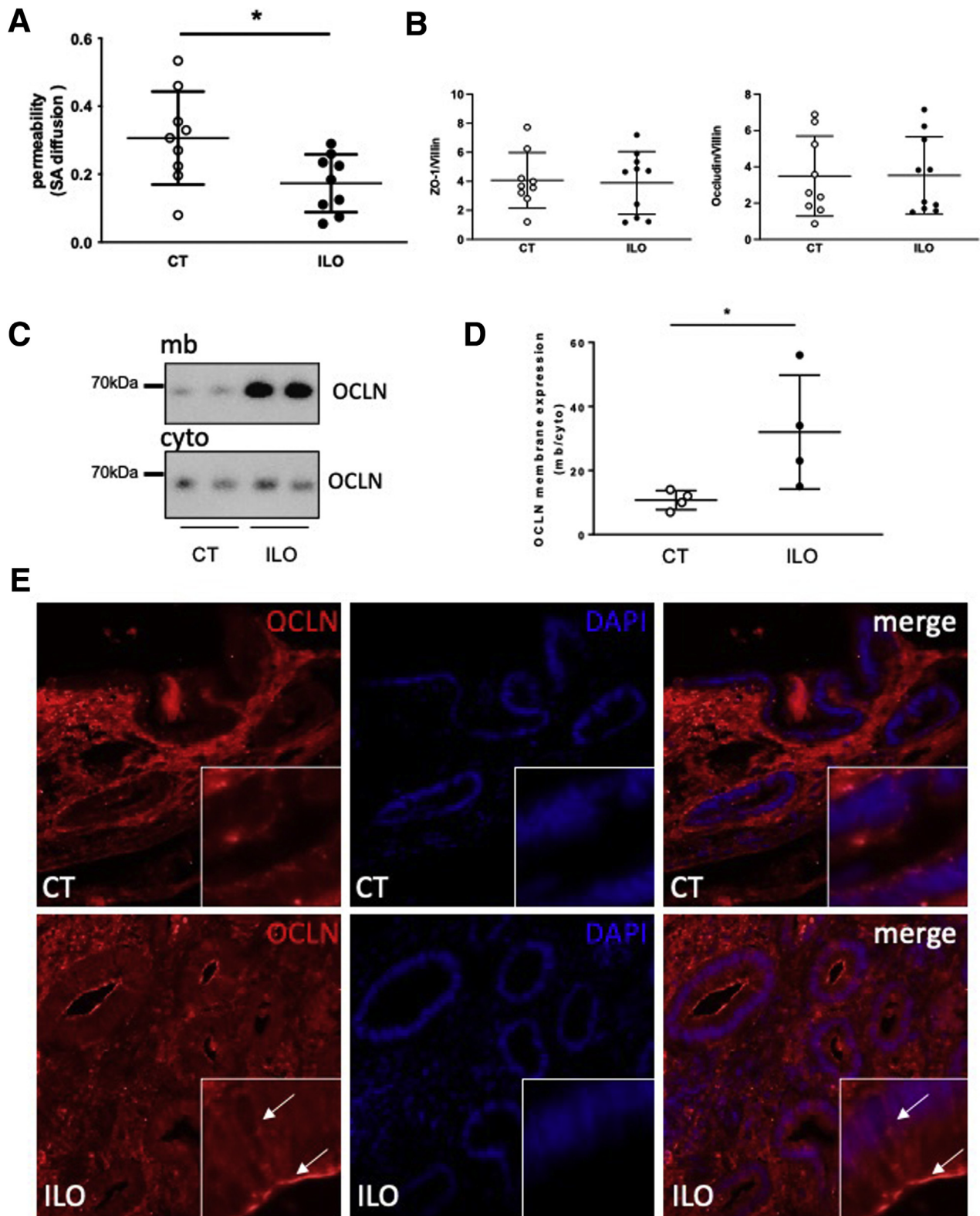


Figure 11. PGI₂ analog iloprost reduces permeability and induces occludin membrane location of biopsies from IBD patients. (A) Paracellular permeability of biopsies from IBD patients measured by sulfonic acid (SA) flux in Ussing chambers after 1-hour pretreatment with 10 μmol/L iloprost (PGI₂) or without (CT). IBD patient (n = 9) data represent the mean SA flux of 2 biopsies per condition per patient. **P* < .05 paired *t* test. (B) Quantification of ZO-1 and occludin expression normalized to villin expression observed by Western blot of biopsies from IBD patients with or without ILO treatment. (C) Occludin membrane (mb) and cytosolic (cyto) expressions were assessed by Western blot after cell fractionation (C) and quantified (D). Data represent means ± SEM of 4 pools of 2 biopsies per group. Nonparametric Mann-Whitney test, **P* < .05. (E) Representative occludin (OCLN) or DAPI staining of human biopsies with or without ILO treatment (scale bar: 50 μm).

Table 1. Main Clinical Features of Patients Used for Biopsy Supernatant Analyses

Patient (n)	Explant location (n)	Age at surgery, y (minimum–maximum)	Sex (M/F)	Treatment received the month before surgery (n)
Control (16)	Colon (16)	45.9 (29–73)	6/10	None (16)
CD (27)	Colon (27)	36.3 (20–48)	16/11	None (2) Anti-TNF (7) Anti-TNF + others ^a (8) Others ^a (10)
UC (19)	Colon (19)	40.6 (21–57)	12/7	None (2) Anti-TNF (3) Anti-TNF + others ^a (3) Others ^a (11)

CD, Crohn's disease; TNF, tumor necrosis factor; UC, ulcerative colitis.

^aImmunosuppressors and/or anti-inflammatory.

gavage and were placed in individual cages. The DAI was calculated on the basis of stool consistency observed during the 4 hours after gavage (0 = hard stool, 1 = soft or liquid stool) and gross bleeding (0 = no blood, 1 = blood) and was composed of scores from 0 to 2. After 4 hours, blood was collected from the tail vein, and paracellular permeability was evaluated by collecting 5 μ L of plasma. The fluorescence of each sample was measured using an automatic microplate reader (Varioskan; Thermo Fisher Scientific, Carlsbad, CA). Transepithelial permeability to HRP was measured by an enzymatic activity assay with 3,3',5,5'-tetramethylbenzidine reagent (BD Bioscience, San Jose, CA). Mice were euthanized, and colon fragments were collected and fixed 1 hour in 4% paraformaldehyde in PBS or snap frozen for further analyses (immunostaining or qPCR). All experiments were approved by the Ethics Committee for Animal Experimentation of Pays de la Loire (study no. 01953.01).

qPCR Analysis

Mucosal fragments from control and IBD patients or colon samples from mice were lysed in RA1 buffer (Macherey-Nagel, Hoerd, France), and total RNA was extracted with a Nucleospin RNAII kit according to the manufacturer's recommendations (Macherey-Nagel). Purified mRNA (1 μ g) was denatured and processed for reverse transcription using Superscript III reverse transcriptase (Invitrogen). PCR amplifications were performed using the Absolute Blue SYBR green fluorescein kit (Roche, Carlsbad, CA) or the Taqman Gene Expression Assay (Life

Technologies) and run on a StepOnePlus system (Life Technologies). The following primers from Life Technologies were used for Taqman assays: IL22 (Mm01226722_g1), IL17a (Mm00439618_m1), IL4 (Mm00445259_m1), IFN- γ (Mm01168134_m1), and ribosomal protein S6 (Mm02342456_g1). Sequences of primers (Sigma-Aldrich) used for SYBR green assays are mentioned in Table 5.

Preparation of Cytosolic and Total Membrane Fractions

Membrane and cytosolic fractions were obtained as previously described.⁸⁹ Briefly, mouse explants or biopsies were harvested in 400 μ L of buffer A (10 mmol/L HEPES, pH 7.9, 1.5 mmol/L MgCl₂, 10 mmol/L KCl, 0.5 mmol/L dithiothreitol), and after 10 strokes in a syringe with a G25 needle, homogenates were centrifuged for 10 minutes at 2000 rpm. A 0.11 volume of buffer B (0.3 mol/L HEPES, pH 7.9, 0.3 mol/L MgCl₂, 1.4 mol/L KCl) was then added to the carefully decanted supernatants and centrifuged for 60 minutes at 100,000g. The high-speed pellet represents the "membrane fraction," and the high-speed supernatant represents the "cytosolic fraction." The membrane fractions were washed twice and resuspended in 1 \times Laemli buffer. Then Laemli was added to the cytosolic fractions, and all fractions were denatured at 95°C for 10 minutes and then put on ice before Western blotting analysis.

Western Blotting

Mucosal fragments from control and IBD patients or colon samples from mice were lysed in RA1 buffer

Table 2. Main Clinical Features of Patients Used for Explants

Patient (n)	Explant location (n)	Age at surgery, y (minimum–maximum)	Sex (M/F)	Treatment at time of surgery (n)
Control, cancer at a distance from tumor (2), other (2)	Colon (4)	63 (48–83)	2/2	None (3) Immunosuppressors (1)

Table 3. Main Clinical Features of Patients Used for Mucosa Molecular Analyses

Patient (n)	Explant location (n)	Age at surgery, y (minimum–maximum)	Sex (M/F)	Treatment at time of surgery (n)
Control, cancer at a distance from tumor (20)	Ileum (4) Colon (15) Rectum (1)	61.8 (38–82)	14/6	None (19) Radiotherapy (1)
CD (20)	Ileum (8) Colon (12) Rectum (0)	37.4 (17–63)	9/11	None (7) Mesalamine (1) IS (4) MTT + IS (1) Anti-TNF (6) Anti-TNF+IS (1)
UC (16)	Ileum (2) Colon (11) Rectum (3)	43 (19–60)	8/8	None (11) Mesalamine (1) IS (0) MTT + IS (0) Anti-TNF (4) Anti-TNF+IS (0)

CD, Crohn's disease; IS, immunosuppressors; MTT, methotrexate; TNF, tumor necrosis factor; UC, ulcerative colitis.

(Macherey-Nagel), and total protein extraction was performed with a Nucleospin RNAII kit according to the manufacturer's recommendations. For Caco-2 filters, cells were washed with ice-cold PBS and lysed in ice-cold RIPA buffer complete with protease inhibitor (Roche) and serine-threonine phosphatase inhibitor (Sigma-Aldrich) cocktails. Nuclei and intact cells were removed by centrifugation at 10,000g for 10 minutes at 4°C. Samples were processed for electrophoresis using an MES Sodium Dodecyl Sulfate buffer kit (Invitrogen). Samples were separated on 4%–12% Bis-Tris or 3%–8% Tris-Acetate gels (Life Technologies). Proteins were transferred to nitrocellulose membranes with the iBlot system (Life Technologies). After blocking with Tris-buffered saline/0.1% Tween-20/5% nonfat dry milk for 30 minutes, blots were incubated overnight at 4°C with the following primary antibodies diluted in Tris-buffered saline/5% nonfat dry milk: mouse anti-ZO-1 (1:200; Thermo Fisher Scientific), rabbit anti-occludin (1:500; Abcam, Cambridge, UK), rabbit anti-junctional adhesion molecule-A (1:500; Bethyl Laboratories, Montgomery, TX), rabbit anti-claudin-2

(1:200; Life Technologies), rabbit anti-cingulin (1:500; Santa Cruz Biotechnology, Dallas, TX), mouse anti-phospho-MLC20 (1:200; Cell Signaling Technology, Danvers, MA), rabbit anti-PCNA (1:500; Abcam), rabbit anti-phospho-Akt and anti-Akt (1:400; Cell Signaling Technology), rabbit anti-cleaved caspase-3 (1:200; Cell Signaling Technology), and mouse anti- β -actin (1:10,000; Sigma-Aldrich). Immunoblots were probed with the appropriate HRP-conjugated secondary antibodies (Life Technologies) and visualized by chemiluminescence (Bio-Rad, Hercules, CA) using a Gel-Doc imager and Image Lab Software (Bio-Rad). The value of protein immunoreactivity was normalized to β -actin immunoreactivity and expressed as the fold-increase relative to the average of control values taken as 1.

Immunohistochemistry and Histopathology

Formalin-fixed human and mice tissues were embedded in paraffin using an embedding station (LEICA EG1150C, Wetzlar, Germany) and cut into 3- μ m sections using a microtome (LEICA RM2255).

Table 4. Main Clinical Features of Patients Used for Biopsy Permeability Analyses

Patient (n)	Explant localization (n)	Age at surgery, y (minimum–maximum)	Sex (M/F)	Treatment at time of surgery (n)
CD (7), UC (2)	Ileum (4) Colon (14) Rectum (0)	32.7 (17–63)	5/4	None (0) Mesalamine (1) IS (1) MTT+IS (1) Anti-TNF (3) Anti-TNF+IS (3)

CD, Crohn's disease; IS, immunosuppressors; MTT, methotrexate; TNF, tumor necrosis factor; UC, ulcerative colitis.

Table 5. Sequences of Primers Used for SYBR Green Assays

Prostaglandin I2 Receptor (IP, PTGIR) #NM_000960.3
Forward Primer: 5'-CTCTCACGATCCGCTGCTTC-3'
Reverse Primer: 5'-GAGCTGGGAAAGGGGTGTCT-3'
Tumor necrosis factor alpha (TNF α) # NM_013693.3
Forward Primer: 5'-GAACTTCGGGTGATCGGTCC-3'
Reverse Primer: 5'-GCCACTCCAGTCTCTCC-3'
Interleukin 1 beta (IL1 β) # NM_008361.4
Forward Primer : 5'-GCCTCGTGTCTCGGACCCATA-3'
Reverse Primer : 5'-TTGAGGCCCAAGGCCACAGGT-3'
Interleukin 6 (IL6) #NM_031168.2
Forward Primer : 5'-TCCAGTTGCCTTCTGGGAC-3'
Reverse Primer : 5'-AGTCTCCTCCGGACTTGT-3'
Ribosomal protein S6 (RPS6) # NM_001010.2
Forward Primer : 5'-CCAAGCTTATTACAGCTCTTGTACTCC-3'
Reverse Primer: 5'-CCCTCGAGTCCCTCATTCTTTGGC-3'

Fluorescence

Slides were deparaffinized with 2 xylene baths (5 minutes each) and incubated in 4 ethanol baths (100%, 95%, 70%, and 70%, respectively; 3 minutes each). After a rinse in distilled water, slides were washed in PBS, and antigen retrieval was performed using a sodium citrate solution (2.94 g sodium citrate tribasic, 1 L distilled water, 500 μ L Tween-20, pH 6) at 95°C for 20 minutes. Slides were incubated in 100 mmol/L NH₄Cl for 15 minutes before incubation in PBS/0.5% Triton X-100 for 1 hour and blocking for 2 hours in 10% horse serum in PBS/0.5% Triton X-100. Primary antibodies for cleaved caspase-3 (1:100; rabbit polyclonal, 9661; Cell Signaling Technology), cytodeath M30 (1:100; Roche), or occludin (1:100; rabbit polyclonal, Abcam) were incubated on slides overnight at 4°C before incubating with the appropriate secondary antibody for 2 hours at room temperature. Images were acquired with an Olympus IX 50 or Zeiss Axio Observer fluorescence microscope coupled to a digital camera (model DP71, Olympus, Tokyo, Japan or Hamamatsu Photonics, Hamamatsu, Japan) and analyzed with Cell B software (Soft Imaging System; Olympus) or Zen software. The fluorescence of the mucosal area was reported to estimate cleaved caspase-3 expression using ImageJ software (National Institutes of Health, Bethesda, MD).

Histologic Score

Hematein Phloxin Safran coloration allowed the visualization of tissue morphology. Tissue damage was scored in a blinded manner by quantifying destruction of mucosal architecture, cellular infiltration, muscle thickening, and loss of goblet cells. The extent of destruction of normal mucosal architecture was scored as 0–3 (0 = no destruction, 1 = 1/3 basal destruction, 2 = 2/3 basal destruction, 3 = loss of crypt and epithelium). The presence and degree of cellular infiltration were also scored as 0–3 when the infiltration was normal, around the crypt basis, reaching the muscularis mucosae, and reaching the submucosa, respectively. The extent of muscle thickening was scored as 0–3 when the thickening was none, mild, moderate, or massive, respectively. The presence or

absence of goblet cell depletion was scored as 0 (normal) or 1 (massive depletion). An extension factor of 1–4 was applied when the criteria measured reached 25%, 50%, 75%, or 100% of the fragment analyzed.

Mouse Colonic Explants

Colons from C57BL/6 NRJ mice were removed and washed 3 times in cold Krebs's solution. For immunostaining, colon pieces were incubated with biopsy medium (Dulbecco modified Eagle medium containing 4.5 g/L glucose, 2.5% fetal bovine serum, 100 IU/mL penicillin, 100 μ g/mL streptomycin, 20 μ g/mL gentamycin, and 1.1 μ g/mL AmphoB) containing 10 μ mol/L iloprost at 37°C with 95% O₂ and 5% CO₂. After 1 hour, 1 μ mol/L staurosporine (Promocell, Heidelberg, Germany) was added to colon segments for 2 hours before fixing tissues for 1 hour in 4% paraformaldehyde in PBS. Apoptosis scores were assessed on these samples by quantifying cells positive for cleaved caspase-3 staining. The extent of apoptosis was scored as 0–2 (0 = no positive cells, 1 = 1/2 positive basal cells, 2 = positivity along the entire crypt). An extended score factor of 1–4 was applied when positivity reached 25%, 50%, 75%, or 100% of the fragment analyzed, respectively. For the paracellular permeability measurement, 8 pieces of each colon were incubated with biopsy medium containing 1–100 μ mol/L iloprost (Figure 7) as described earlier. After 4 hours, 1 μ mol/L staurosporine was added to colon segments and incubated overnight. Twenty-four hours after the start of the incubation process, colon pieces were mounted in Ussing chambers, and paracellular permeability was measured as detailed above.

Ex Vivo Permeability Assessment in Ussing Chambers

Human biopsies and human or mice explants were mounted in Ussing chambers (0.011 or 0.03 cm² exposed surface area, respectively; Physiologic Instruments, San Diego, CA) as previously described.⁹⁰ Each chamber contained 2 mL of Ham's/F12 medium (Invitrogen) maintained at 37°C and continuously gassed with 95% O₂ and 5% CO₂. After 30 minutes of equilibration, 200 μ L of apical medium was replaced by 200 μ L of fluorescein–5.6 sulfonic acid (1 mg/mL). The fluorescence level of basolateral aliquots (150 μ L) was measured every 30 minutes for a period of 180 minutes to evaluate paracellular permeability using a Variskan automatic microplate reader. Samples were then used for preparation of cytosolic and total membrane fractions and further Western blotting analysis.

Drugs

Iloprost and epoprostenol have different selectivity for prostanoid receptors. Iloprost can bind to and activate EP1 with greater affinity than IP, and epoprostenol can bind to and activate EP3 receptors with 20 times less affinity than IP.⁸⁰ The methyl acetate in which iloprost was supplied was evaporated under a gentle stream of nitrogen and immediately resuspended in dimethyl sulfoxide to

2359 obtain a 10 or 100 mmol/L stock solution. The same
2360 dilution of dimethyl sulfoxide alone was always used in
2361 control wells.

2362 Statistics

2364 Except for PUFA-metabolite profiling, all graphics were
2365 drawn and analyzed using GraphPad Prism 5.0 Software
2366 (GraphPad Software, La Jolla, CA). Values are expressed as
2367 means \pm standard error of the mean (SEM). The significance
2368 of differences was determined using either 2-way ANOVA
2369 followed by Bonferroni post hoc test or nonparametric
2370 Mann-Whitney test using GraphPad Prism 5.0. Statistical
2371 significance was reached when $P < .05$. For PUFA-metabolite
2372 profiling, 1-way ANOVA was performed using [www.
2373 metaboanalyst.ca](http://www.metaboanalyst.ca) with an adjusted P value cutoff of .05
2374 and a Fisher least significant difference post hoc test.

2376 References

- 2377 1. Molodecky NA, Soon IS, Rabi DM, Ghali WA, Ferris M,
2378 Chernoff G, Benchimol EI, Panaccione R, Ghosh S,
2379 Barkema HW, Kaplan GG. Increasing incidence and
2380 prevalence of the inflammatory bowel diseases with
2381 time, based on systematic review. *Gastroenterology*
2382 2012;142:46–54 e42, quiz e30.
- 2383 2. Ananthakrishnan AN. Epidemiology and risk factors for
2384 IBD. *Nature Reviews Gastroenterology Hepatology* 2015;
2385 12:205–217.
- 2386 3. Gu YB, Zhong J. Endoscopic management of stricturing
2387 Crohn's disease. *J Dig Dis* 2020;21:351–354.
- 2388 4. Spinelli A, Armuzzi A, Ciccocioppo R, Danese S,
2389 Gionchetti P, Luglio G, Orlando A, Rispo A, Rizzello F,
2390 Sofo L, Solina G, Poggioli G. Management of patients
2391 with complex perianal fistulas in Crohn's disease:
2392 optimal patient flow in the Italian clinical reality. *Dig Liver*
2393 *Dis* 2020;52:506–515.
- 2394 5. Xavier RJ, Podolsky DK. Unravelling the pathogenesis of
2395 inflammatory bowel disease. *Nature* 2007;448:427–434.
- 2396 6. Khor B, Gardet A, Xavier RJ. Genetics and pathogenesis
2397 of inflammatory bowel disease. *Nature* 2011;
2398 474:307–317.
- 2399 7. Arrieta MC, Bistriz L, Meddings JB. Alterations in in-
2400 testinal permeability. *Gut* 2006;55:1512–1520.
- 2401 8. Okamoto R, Watanabe M. Cellular and molecular
2402 mechanisms of the epithelial repair in IBD. *Dig Dis Sci*
2403 2005;50(Suppl 1):S34–S38.
- 2404 9. Arrieta MC, Madsen K, Doyle J, Meddings J. Reducing
2405 small intestinal permeability attenuates colitis in the *Il10*
2406 gene-deficient mouse. *Gut* 2009;58:41–48.
- 2407 10. Irvine EJ, Marshall JK. Increased intestinal permeability
2408 precedes the onset of Crohn's disease in a subject with
2409 familial risk. *Gastroenterology* 2000;119:1740–1744.
- 2410 11. Arnett ID, Kingstone K, Ghosh S. Abnormal intestinal
2411 permeability predicts relapse in inactive Crohn disease.
2412 *Scand J Gastroenterol* 2000;35:1163–1169.
- 2413 12. Wyatt J, Vogelsang H, Hubl W, Waldhoer T, Lochs H.
2414 Intestinal permeability and the prediction of relapse in
2415 Crohn's disease. *Lancet* 1993;341:1437–1439.
- 2416 13. Soderholm JD, Peterson KH, Olaison G, Franzen LE,
2417 Westrom B, Magnusson KE, Sjobahl R. Epithelial

- permeability to proteins in the noninflamed ileum of 2418
Crohn's disease? *Gastroenterology* 1999;117:65–72. 2419
- 2420 14. Baert F, Moortgat L, Van Assche G, Caenepeel P,
2421 Vergauwe P, De Vos M, Stokkers P, Hommes D,
2422 Rutgeerts P, Vermeire S, D'Haens G. Mucosal healing
2423 predicts sustained clinical remission in patients with
2424 early-stage Crohn's disease. *Gastroenterology* 2010;
2425 138:463–468, quiz e410–e461.
 - 2426 15. Okamoto R, Watanabe M. Role of epithelial cells in the
2427 pathogenesis and treatment of inflammatory bowel dis-
2428 ease. *J Gastroenterol* 2016;51:11–21.
 - 2429 16. Sharon P, Ligumsky M, Rachmilewitz D, Zor U. Role of
2430 prostaglandins in ulcerative colitis: enhanced production
2431 during active disease and inhibition by sulfasalazine.
2432 *Gastroenterology* 1978;75:638–640.
 - 2433 17. Shannon VR, Stenson WF, Holtzman MJ. Induction of
2434 epithelial arachidonate 12-lipoxygenase at active sites of
2435 inflammatory bowel disease. *Am J Physiol* 1993;
2436 264:G104–G111.
 - 2437 18. Ikehata A, Hiwatashi N, Kinouchi Y, Yamazaki H, Ito K,
2438 Toyota T. Altered leukotriene B4 metabolism in colonic
2439 mucosa with inflammatory bowel disease. *Scand J*
2440 *Gastroenterol* 1995;30:44–49.
 - 2441 19. Ligumsky M, Karmeli F, Sharon P, Zor U, Cohen F,
2442 Rachmilewitz D. Enhanced thromboxane a2 and
2443 prostacyclin production by cultured rectal mucosa in
2444 ulcerative colitis and its inhibition by steroids and
2445 sulfasalazine. *Gastroenterology* 1981;81:444–449.
 - 2446 20. Lauritsen K, Staerk Laursen L, Bukhave K, Rask-
2447 Madsen J. Longterm olsalazine treatment: pharmaco-
2448 kinetics, tolerance and effects on local eicosanoid forma-
2449 tion in ulcerative colitis and Crohn's colitis. *Gut* 1988;
2450 29:974–982.
 - 2451 21. Le Loupp AG, Bach-Ngohou K, Bourreille A, Boudin H,
2452 Rolli-Derkinderen M, Denis MG, Neunlist M, Masson D.
2453 Activation of the prostaglandin D2 metabolic pathway
2454 in Crohn's disease: involvement of the enteric nervous
2455 system. *BMC Gastroenterology* 2015;15:112.
 - 2456 22. Hawkey CJ, Karmeli F, Rachmilewitz D. Imbalance of
2457 prostacyclin and thromboxane synthesis in Crohn's
2458 disease. *Gut* 1983;24:881–885.
 - 2459 23. Zifroni A, Treves AJ, Sachar DB, Rachmilewitz D. Pros-
2460 tanoid synthesis by cultured intestinal epithelial and
2461 mononuclear cells in inflammatory bowel disease. *Gut*
2462 1983;24:659–664.
 - 2463 24. Masoodi M, Pearl DS, Eiden M, Shute JK, Brown JF,
2464 Calder PC, Trebble TM. Altered colonic mucosal poly-
2465 unsaturated fatty acid (pufa) derived lipid mediators in ul-
2466 cerative colitis: new insight into relationship with disease
2467 activity and pathophysiology. *PloS One* 2013;8:e76532.
 - 2468 25. Ajuebor MN, Singh A, Wallace JL. Cyclooxygenase-2-
2469 derived prostaglandin D(2) is an early anti-inflammatory
2470 signal in experimental colitis. *Am J Physiol Gastrointest*
2471 *Liver Physiol* 2000;279:G238–G244.
 - 2472 26. Gilroy DW, Colville-Nash PR, McMaster S, Sawatzky DA,
2473 Willoughby DA, Lawrence T. Inducible cyclooxygenase-
2474 derived 15-deoxy(delta)12-14pgj2 brings about acute
2475 inflammatory resolution in rat pleurisy by inducing
2476 neutrophil and macrophage apoptosis. *Faseb J* 2003;
17:2269–2271.

- 2477 27. Hokari R, Kurihara C, Nagata N, Aritake K, Okada Y, Watanabe C, Komoto S, Nakamura M, Kawaguchi A, Nagao S, Urade Y, Miura S. Increased expression of lipocalin-type-prostaglandin D synthase in ulcerative colitis and exacerbating role in murine colitis. *Am J Physiol Gastrointest Liver Physiol* 2011;300:G401–G408. 2536
- 2478 28. Li J, Kong D, Wang Q, Wu W, Tang Y, Bai T, Guo L, Wei L, Zhang Q, Yu Y, Qian Y, Zuo S, Liu G, Liu Q, Wu S, Zang Y, Zhu Q, Jia D, Wang Y, Yao W, Ji Y, Yin H, Nakamura M, Lazarus M, Breyer RM, Wang L, Yu Y. Niacin ameliorates ulcerative colitis via prostaglandin D2-mediated D prostanoid receptor 1 activation. *EMBO Molecular Medicine* 2017;9:571–588. 2537
- 2479 29. Rajakariar R, Hilliard M, Lawrence T, Trivedi S, Colville-Nash P, Bellingan G, Fitzgerald D, Yaqoob MM, Gilroy DW. Hematopoietic prostaglandin D2 synthase controls the onset and resolution of acute inflammation through Pgd2 and 15-deoxydelta12 14 pgj2. *Proc Natl Acad Sci U S A* 2007;104:20979–20984. 2538
- 2480 30. Vong L, Ferraz JG, Panaccione R, Beck PL, Wallace JL. A pro-resolution mediator, prostaglandin D(2), is specifically up-regulated in individuals in long-term remission from ulcerative colitis. *Proc Natl Acad Sci U S A* 2010; 107:12023–12027. 2539
- 2481 31. Gobbetti T, Ducheix S, le Faouder P, Perez T, Riols F, Boue J, Bertrand-Michel J, Dubourdeau M, Guillou H, Perretti M, Vergnolle N, Cenac N. Protective effects of n-6 fatty acids-enriched diet on intestinal ischaemia/reperfusion injury involve lipoxin A4 and its receptor. *Br J Pharmacol* 2015;172:910–923. 2540
- 2482 32. Das UN. Inflammatory bowel disease as a disorder of an imbalance between pro- and anti-inflammatory molecules and deficiency of resolution bioactive lipids. *Lipids in Health and Disease* 2016;15:11. 2541
- 2483 33. Dennis EA, Norris PC. Eicosanoid storm in infection and inflammation. *Nature Reviews Immunology* 2015; 15:511–523. 2542
- 2484 34. Pochard C, Coquenlorge S, Jaulin J, Cenac N, Vergnolle N, Meurette G, Freyssinet M, Neunlist M, RollidKinderen M. Defects in 15-HETE production and control of epithelial permeability by human enteric glial cells from patients with Crohn's disease. *Gastroenterology* 2016;150:168–180. 2543
- 2485 35. Coquenlorge S, Van Landeghem L, Jaulin J, Cenac N, Vergnolle N, Duchalais E, Neunlist M, RollidKinderen M. The arachidonic acid metabolite 11beta-prostaglandinF2alpha controls intestinal epithelial healing: deficiency in patients with Crohn's disease. *Scientific Reports* 2016;6:25203. 2544
- 2486 36. Miyoshi H, VanDussen KL, Malvin NP, Ryu SH, Wang Y, Sonnek NM, Lai CW, Stappenbeck TS. Prostaglandin E2 promotes intestinal repair through an adaptive cellular response of the epithelium. *EMBO J* 2017;36:5–24. 2545
- 2487 37. Herminghaus A, Eberhardt R, Truse R, Schulz J, Bauer I, Picker O, Vollmer C. Nitroglycerin and iloprost improve mitochondrial function in colon homogenate without altering the barrier integrity of Caco-2 monolayers. *Frontiers in Medicine* 2018;5:291. 2546
- 2488 38. Leers MP, Kolgen W, Bjorklund V, Bergman T, Tribbick G, Persson B, Bjorklund P, Ramaekers FC, Bjorklund B, Nap M, Jornvall H, Schutte B. Immunocytochemical detection and mapping of a cytokeratin 18 neo-epitope exposed during early apoptosis. *J Pathol* 1999;187:567–572. 2547
- 2489 39. Lee JY, Wasinger VC, Yau YY, Chuang E, Yajnik V, Leong RW. Molecular pathophysiology of epithelial barrier dysfunction in inflammatory bowel diseases. *Proteomes* 2018;6:17. 2548
- 2490 40. Ricciotti E, FitzGerald GA. Prostaglandins and inflammation. *Arterioscler Thromb Vasc Biol* 2011; 31:986–1000. 2549
- 2491 41. Sinzinger H, Silberbaver K, Seyfried H. Rectal mucosa prostacyclin formation in ulcerative colitis. *Lancet* 1979; 1:444. 2550
- 2492 42. Seyfried H, Sinzinger H, Silberbauer K. [prostacyclin (PGI2) activity in the rectal mucosa of patients with ulcerative colitis (author's transl)]. *Wien Klin Wochenschr* 1980;92:282–284. 2551
- 2493 43. Tihanyi K, Rozsa I, Banai J, Dobo I, Bajtai A. Tissue concentrations and correlations of prostaglandins in healthy and inflamed human esophageal and jejunal mucosa. *J Gastroenterol* 1996;31:149–152. 2552
- 2494 44. Rehal S, von der Weid PY. Experimental ileitis alters prostaglandin biosynthesis in mesenteric lymphatic and blood vessels. *Prostaglandins Other Lipid Mediat* 2015; 116–117:37–48. 2553
- 2495 45. Sadler T, Bhasin JM, Xu Y, Barnholz-Sloan J, Chen Y, Ting AH, Stylianou E. Genome-wide analysis of DNA methylation and gene expression defines molecular characteristics of Crohn's disease-associated fibrosis. *Clinical Epigenetics* 2016;8:30. 2554
- 2496 46. Whittle BJ. Inhibition of prostacyclin (PGI2) formation in the rat small-intestine and gastric mucosa by the ulcerogen, indomethacin [proceedings]. *Br J Pharmacol* 1978; 64:438P. 2555
- 2497 47. Robert A. Experimental production of duodenal ulcers. *Biol Gastroenterol (Paris)* 1974;7:145–161. 2556
- 2498 48. Sharon P, Cohen F, Zifroni A, Karmeli F, Ligumsky M, Rachmilewitz D. Prostanoid synthesis by cultured gastric and duodenal mucosa: possible role in the pathogenesis of duodenal ulcer. *Scand J Gastroenterol* 1983;18:1045–1049. 2557
- 2499 49. Hillier K, Smith CL, Jewell R, Arthur MJ, Ross G. Duodenal mucosa synthesis of prostaglandins in duodenal ulcer disease. *Gut* 1985;26:237–240. 2558
- 2500 50. Robert A, Schultz JR, Nezamis JE, Lancaster C. Gastric antisecretory and antiulcer properties of PGE2, 15-methyl PGE2, and 16, 16-dimethyl PGE2: intravenous, oral and intrajejunal administration. *Gastroenterology* 1976;70:359–370. 2559
- 2501 51. Cohen MM. Mucosal cytoprotection by prostaglandin E2. *Lancet* 1978;2:1253–1254. 2560
- 2502 52. Peng X, Li J, Tan S, Xu M, Tao J, Jiang J, Liu H, Wu B. Cox-1/PGE2/EP4 alleviates mucosal injury by upregulating beta-arr1-mediated Akt signaling in colitis. *Scientific Reports* 2017;7:1055. 2561
- 2503 53. Stenson WF. Prostaglandins and epithelial response to injury. *Current Opinion in Gastroenterology* 2007; 23:107–110. 2562
- 2504 54. Bach-Ngohou K, Mahe MM, Aubert P, Abdo H, Boni S, Bourreille A, Denis MG, Lardeux B, Neunlist M, 2563

- 2595 Masson D. Enteric glia modulate epithelial cell proliferation and differentiation through 15-deoxy-12,14-prostaglandin J₂. *J Physiol* 2010;588:2533–2544. 2655
- 2596 55. Ruwart MJ, Rush BD. Prostacyclin inhibits gastric emptying and small-intestinal transit in rats and dogs. 2656
- 2597 *Gastroenterology* 1984;87:392–395. 2657
- 2598 56. Bennett A, Sanger GJ. Prostacyclin relaxes the longitudinal muscle of human isolated stomach and antagonizes contractions to some prostanoids [proceedings]. 2658
- 2599 *J Physiol* 1980;298:45P–46P. 2659
- 2600 57. Sanger GJ, Bennett A. Regional differences in the responses to prostanoids of circular muscle from guinea-pig isolated intestine. *J Pharm Pharmacol* 1980; 2660
- 2601 32:705–708. 2661
- 2602 58. Thor P, Konturek JW, Konturek SJ, Anderson JH. Role of prostaglandins in control of intestinal motility. *Am J Physiol* 1985;248:G353–G359. 2662
- 2603 59. Vermue NA, Den Hertog A, Zaagsma J. Desensitization of PGE₂ and PGI₂ induced contractions in different smooth muscles of guinea-pig unmasking relaxing properties of prostanoids. *Eur J Pharmacol* 1987; 2663
- 2604 144:399–403. 2664
- 2605 60. Paustian PW, Chapnick BM, Feigen LP, Hyman AL, Kadowitz PJ. Effects of 13, 14-dehydroprostacyclin methyl ester on the feline intestinal vascular bed. *Prostaglandins* 1977;14:1141–1152. 2665
- 2606 61. Crane BH, Maish TL, Maddox YT, Corey EJ, Szekely I, Ramwell PW. Effect of prostaglandin I₂ and analogs on platelet aggregation and smooth muscle contraction. *J Pharmacol Exp Ther* 1978;206:132–138. 2666
- 2607 62. Ogawa H, Rafiee P, Fisher PJ, Johnson NA, Otterson MF, Binion DG. Sodium butyrate inhibits angiogenesis of human intestinal microvascular endothelial cells through Cox-2 inhibition. *FEBS Lett* 2003;554:88–94. 2667
- 2608 63. Raptis D, Pramateftakis MG, Kanellos I. Our 20-year experience with experimental colonic anastomotic healing. *Journal of Medicine and Life* 2018;11:5–14. 2668
- 2609 64. Bostanoglu S, Dincer S, Keskin A, Bostanoglu A, Dursun A, Serim C. Beneficial effect of iloprost on impaired colonic anastomotic healing induced by intraperitoneal 5-fluorouracil infusion. *Dis Colon Rectum* 1998;41:642–648. 2669
- 2610 65. Sakaguchi T, Nakamura S, Suzuki S, Baba S, Nakashima M. Endogenous endotoxemia after massive hepatectomy and portal vein stenosis: beneficial effect of a prostaglandin I₂ analogue on intestinal permeability. *Eur Surg Res* 1996;28:341–350. 2670
- 2611 66. Konturek SJ, Brzozowski T, Radecki T, Pastucki I. Comparison of gastric and intestinal antisecretory and protective effects of prostacyclin and its stable thiaimino-analogue (hoe 892) in conscious rats. *Prostaglandins* 1984;28:443–453. 2671
- 2612 67. Dembinski A, Konturek SJ. Effects of E, F, and I series prostaglandins and analogues on growth of gastroduodenal mucosa and pancreas. *Am J Physiol* 1985; 2672
- 2613 248:G170–G175. 2673
- 2614 68. Blikslager AT, Roberts MC, Argenzio RA. Prostaglandin-induced recovery of barrier function in porcine ileum is triggered by chloride secretion. *Am J Physiol* 1999; 2674
- 2615 276:G28–G36. 2675
- 2616 69. Blume ED, Taylor CT, Lennon PF, Stahl GL, Colgan SP. Activated endothelial cells elicit paracrine induction of epithelial chloride secretion: 6-keto-PGF₁α is an epithelial secretagogue. *J Clin Invest* 1998; 2676
- 2617 102:1161–1172. 2677
- 2618 70. Moriarty KJ, O'Grady J, Rolston DD, Kelly MJ, Clark ML. Effect of prostacyclin (PGI₂) on water and solute transport in the human jejunum. *Gut* 1986;27:158–163. 2678
- 2619 71. Goerg KJ, Wanitschke R, Becker U, Meyer zum Buschenfelde KH. Effect of the stable prostacyclin analogue iloprost on water and electrolyte transfer of the rat ileum and colon in vivo. *Eur J Clin Invest* 1988; 2679
- 2620 18:124–127. 2680
- 2621 72. Qiao L, Kozoni V, Tsioulis GJ, Koutsos MI, Hanif R, Shiff SJ, Rigas B. Selected eicosanoids increase the proliferation rate of human colon carcinoma cell lines and mouse colonocytes in vivo. *Biochim Biophys Acta* 1995; 2681
- 2622 1258:215–223. 2682
- 2623 73. Cutler NS, Graves-Deal R, LaFleur BJ, Gao Z, Boman BM, Whitehead RH, Terry E, Morrow JD, Coffey RJ. Stromal production of prostacyclin confers an antiapoptotic effect to colonic epithelial cells. *Cancer Res* 2003;63:1748–1751. 2683
- 2624 74. Zushi S, Shinomura Y, Kiyohara T, Minami T, Sugimachi M, Higashimoto Y, Kanayama S, Matsuzawa Y. Role of prostaglandins in intestinal epithelial restitution stimulated by growth factors. *Am J Physiol* 1996;270:G757–G762. 2684
- 2625 75. Blikslager AT, Zimmel DN, Young KM, Campbell NB, Little D, Argenzio RA. Recovery of ischaemic injured porcine ileum: evidence for a contributory role of Cox-1 and Cox-2. *Gut* 2002;50:615–623. 2685
- 2626 76. Campbell NB, Blikslager AT. The role of cyclooxygenase inhibitors in repair of ischaemic-injured jejunal mucosa in the horse. *Equine Vet J Suppl* 2000:59–64. 2686
- 2627 77. Tan XD, Chen YH, Liu QP, Gonzalez-Crussi F, Liu XL. Prostanoids mediate the protective effect of trefoil factor 3 in oxidant-induced intestinal epithelial cell injury: role of cyclooxygenase-2. *J Cell Sci* 2000;113(Pt 12):2149–2155. 2687
- 2628 78. Little D, Dean RA, Young KM, McKane SA, Martin LD, Jones SL, Blikslager AT. PI3K signaling is required for prostaglandin-induced mucosal recovery in ischemia-injured porcine ileum. *Am J Physiol Gastrointest Liver Physiol* 2003;284:G46–G56. 2688
- 2629 79. Moreno JJ. Eicosanoid receptors: targets for the treatment of disrupted intestinal epithelial homeostasis. *Eur J Pharmacol* 2017;796:7–19. 2689
- 2630 80. Clapp LH, Gurung R. The mechanistic basis of prostacyclin and its stable analogues in pulmonary arterial hypertension: role of membrane versus nuclear receptors. *Prostaglandins Other Lipid Mediat* 2015; 2690
- 2631 120:56–71. 2691
- 2632 81. Turner JR. Intestinal mucosal barrier function in health and disease. *Nature Reviews Immunology* 2009; 2692
- 2633 9:799–809. 2693
- 2634 82. Gitter AH, Wullstein F, Fromm M, Schulzke JD. Epithelial barrier defects in ulcerative colitis: characterization and quantification by electrophysiological imaging. *Gastroenterology* 2001;121:1320–1328. 2694
- 2635 2695
- 2636 2696
- 2637 2697
- 2638 2698
- 2639 2699
- 2640 2700
- 2641 2701
- 2642 2702
- 2643 2703
- 2644 2704
- 2645 2705
- 2646 2706
- 2647 2707
- 2648 2708
- 2649 2709
- 2650 2710
- 2651 2711
- 2652 2712
- 2653 2713

- 2713 83. Yu LC, Flynn AN, Turner JR, Buret AG. SglT-1-mediated
2714 glucose uptake protects intestinal epithelial cells against
2715 LPS-induced apoptosis and barrier defects: a novel
2716 cellular rescue mechanism? *Faseb J* 2005;19:1822–1835.
- 2717 84. Su L, Nalle SC, Shen L, Turner ES, Singh G, Breskin LA,
2718 Khramtsova EA, Khramtsova G, Tsai PY, Fu YX,
2719 Abraham C, Turner JR. TNFR2 activates MLCK-
2720 dependent tight junction dysregulation to cause
2721 apoptosis-mediated barrier loss and experimental colitis.
2722 *Gastroenterology* 2013;145:407–415.
- 2723 85. Rodriguez-Roisin R, Bartolome SD, Huchon G,
2724 Krowka MJ. Inflammatory bowel diseases, chronic liver
2725 diseases and the lung. *Eur Respir J* 2016;47:638–650.
- 2726 86. Birukova AA, Zagranichnaya T, Fu P, Alekseeva E,
2727 Chen W, Jacobson JR, Birukov KG. Prostaglandins
2728 PGE(2) and PGI(2) promote endothelial barrier enhance-
2729 ment via PKA- and Epac1/Rap1-dependent Rac activa-
2730 tion. *Exp Cell Res* 2007;313:2504–2520.
- 2731 87. Le Faouder P, Baillif V, Spreadbury I, Motta JP,
2732 Rousset P, Chene G, Guigne C, Terce F, Vanner S,
2733 Vergnolle N, Bertrand-Michel J, Dubourdeau M,
2734 Cenac N. LC-MS/MS method for rapid and concomitant
2735 quantification of pro-inflammatory and pro-resolving
2736 polyunsaturated fatty acid metabolites. *J Chromatogr B
2737 Analyt Technol Biomed Life Sci* 2013;932:123–133.
- 2738 88. Xia M, Zhu Y. Signaling pathways of ATP-induced PGE2
2739 release in spinal cord astrocytes are EGFR trans-
2740 activation-dependent. *Glia* 2011;59:664–674.
- 2741 89. Rolli-Derkinderen M, Toumaniantz G, Pacaud P,
2742 Loirand G. RhoA phosphorylation induces Rac1 release
2743 from guanine dissociation inhibitor alpha and stimulation
2744 of vascular smooth muscle cell migration. *Mol Cell Biol*
2745 2010;30:4786–4796.
- 2746 90. De Quelen F, Chevalier J, Rolli-Derkinderen M, Mourot J,
2747 Neunlist M, Boudry G. N-3 polyunsaturated fatty acids in
2748 the maternal diet modify the postnatal development of
2749 nervous regulation of intestinal permeability in piglets.
2750 *J Physiol* 2011;589:4341–4352.
- 2751
2752
2753
2754
2755
2756
2757
2758
2759
2760
2761
2762
2763
2764
2765
2766
-
- Received May 12, 2020. Accepted May 3, 2021.
- Correspondence**
Address correspondence to: Malvyne Rolli-Derkinderen, PhD, Inserm UMR1235, The Enteric Nervous System in Gut and Brain Disorders TENS, School of Medicine, University of Nantes, 1 Rue Gaston Veil, Nantes F-44035, France. e-mail: malvyne.derkinderen@univ-nantes.fr; fax: XXX.
- Acknowledgments**
The authors thank Tony Durand for qPCR expertise and Emilie Durieu for human biocollection management. Experiments were carried out within the small animal exploration facility Therassay, which is supported by the GIS-IBiSA program. The authors also thank Guylène Hamery and Julie Pajot for their great help in animal facility organization, the CIC 1413, the CCDE, and the Department of Pathological Anatomy and Cytology of the Hôtel-Dieu-Nantes hospital for their involvement. They acknowledge the Toulouse INSERM Metatoul-Lipidomique Core Facility-MetaboHub where lipidomic analyses were performed.
- CRedit Authorship Contributions**
Camille Pochard (Formal analysis: Equal; Investigation: Lead; Methodology: Equal; Writing – original draft: Equal)
Jacques Gonzales (Investigation: Equal; Methodology: Supporting)
Anne Bessard (Investigation: Supporting; Writing – review & editing: Supporting)
Maxime Mickael Mahe (Methodology: Supporting; Writing – review & editing: Supporting)
Arnaud Bourreille (Data curation: Equal; Investigation: Supporting; Resources: Equal)
Nicolas Cenac (Data curation: Equal; Investigation: Supporting; Writing – review & editing: Supporting)
Anne Jarry (Data curation: Supporting; Methodology: Supporting; Writing – review & editing: Supporting)
Emmanuel Coron (Data curation: Supporting; Resources: Supporting)
Juliette Podevin (Data curation: Supporting; Resources: Supporting)
Guillaume Meurette (Data curation: Supporting; Resources: Supporting)
Michel Neunlist (Conceptualization: Supporting; Formal analysis: Supporting; Funding acquisition: Lead; Project administration: Supporting)
Malvyne Rolli-Derkinderen, PhD (Conceptualization: Lead; Formal analysis: Equal; Investigation: Supporting; Methodology: Equal; Project administration: Lead; Supervision: Lead; Validation: Lead; Writing – original draft: Lead; Writing – review & editing: Lead)
- Conflicts of interest**
The authors disclose no conflicts.
- Funding**
Supported by grants from the INSERM, Nantes University, the Centre Hospitalier Universitaire (CHU) of Nantes, the Agence Nationale de la Recherche (ANR-19-CE14-0023-02), and the SantéDige Foundation. CP is a recipient of a doctoral fellowship from Inserm-Pays de La Loire. MRD is supported by the Centre National pour la Recherche Scientifique (CNRS).
- 2767
2768
2769
2770
2771
2772
Q23
2772
Q4
2773
2774
2775
2776
2777
2778
2779
2780
2781
2782
2783
2784
2785
2786
2787
2788
2789
2790
2791
2792
2793
2794
2795
2796
2797
2798
2799
2800
2801
Q11
2802
2803
2804
2805
2806
2807
2808
2809
2810
2811
2812
2813
2814
2815
2816
2817
2818
2819
2820